CHAPTER 4. SIMULATIONS

Terms Used in this Chapter

Average Deviation – The absolute average between deviations of known x's and known y's.

Calibration – Simulation models are often refined by adjusting parameters and input data to increase model performance.

Correlation Coefficient – R-Squared Value - The Pearson product moment calculated for two data sets. The r-squared value can be interpreted as the proportion of the variance in y attributable to the variance in x.

Heat Source – A stream temperature computer model that is maintained by DEQ.

Potential Daily Solar Load – The solar heat load that would be received without attenuation or scattering from land cover (i.e. in the absence of stream surface shade)

Sample Size (n) – The number of discrete measurements or simulated values

Shade Curve – Effective shade for a particular land cover type, latitude and time period for varying channel width values.

Solar Altitude – The vertical angle of the sun during daytime

Solar Azimuth – The horizontal angle of the sun during daytime

Solar Heat Flux – Rate of heating per unit area from solar radiation. For the purposes of this analysis, the solar heat flux is the rate of heat delivery to the stream water column accounting for topographic shading, atmospheric and land cover attenuation and scattering, surface reflection, and stream transmissivity.

Solar Heat Load – Heat derived from solar radiation per day in a given stream segment. For the purposes of this analysis, the solar heat load is the heat delivered to the stream water column.

Total Solar Heat Load – Total daily heat delivery to the stream in the current condition.

Background Solar Heat Load – An estimate of the solar heat load under potential land cover and channel morphology conditions. This condition implies no anthropogenic warming from nonpoint sources.

Nonpoint Source Solar Heat Load – Derived by subtracting the nonpoint source solar heat load from the total solar heat load.

Simulation Scenario – Running a simulation while changing the values of one or more of the input parameters, such as land cover or channel width.

Solar Radiation – Radiant heat derived from the sun.

Solar Zenith – The mid-day angle at which the sun is highest in the sky.

Standard Error – A measure of the amount of error in the prediction of a value for an individual known value

System Potential – For the purposes of this analysis, potential conditions are defined for both land cover and channel width. *System potential* condition occurs when both land cover and channel width are at potential. This condition implies that a condition of no anthropogenic disturbance.

Transmissivity – A dimensionless value measured as the fraction of incident radiation that is transmitted through the body

TTools – A GIS sampling tool developed and maintained by DEQ used to build input data sets for channel morphology, land cover and FLIR.

Validation – Statistical quantification of simulation model performance.

4.1 Overview of Modeling Purpose, Valid Applications & Limitations

4.1.1 Channel Morphology Analysis

Modeling Purpose

- Quantify existing Rosgen channel types and morphologic parameters.
- Develop a methodology to estimate a potential equilibrium condition for channel morphology.
- Establish threshold near stream disturbance zone (NSDZ) widths for the stream network, above which channel conditions are considered to deviate from a potential equilibrium condition.

Valid Applications

- Estimate near stream disturbance zone width as a function of drainage area and Rosgen channel type.
- Identify site-specific deviations of current condition near stream disturbance zone width from threshold potential conditions.

Limitations

- Many areas within the North Coast Subbasins were not analyzed. This analytical effort provides site specific near stream disturbance zone width targets for mapped streams within the Nehalem River subbasin only. Therefore, streams in the Necanicum, Lower Columbia, and Clatskanie River subbasins have no site specific near stream disturbance zone widths presented in this TMDL.
- All applications of the channel morphology analytical methods should consider validation statistics presented in **Section 3.4 Channel Morphology**.

4.1.2 Near Stream Land Cover Analysis

Modeling Purpose

- Quantify existing near stream land cover types and physical attributes.
- Develop a methodology to estimate potential conditions for near stream land cover.
- Establish threshold near stream land cover type and physical attributes for the stream network, below which land cover conditions are considered to deviate from a potential condition.

Valid Applications

- Estimate current condition near stream land cover type and physical attributes.
- Estimate potential condition near stream land cover type and physical attributes.
- Identify site-specific deviations of current near stream land cover conditions from threshold potential conditions.

Limitations

- Methodology is based on ground level and GIS data such as, vegetation surveys, and digitized polygons from air photos. Each data source has accuracy considerations.
- Associations used for land cover classification are assigned median values to describe physical attributes, and in some cases, this methodology significantly underestimates landscape variability.

4.1.3 Hydrology Analysis

Modeling Purpose

- Map and quantify surface and subsurface flow inputs and withdrawal outputs.
- Develop a mass balance for the stream network by quantify existing instream flow volume
- Quantify average velocity and average stream depth as a function of flow volume, stream gradient, average channel width and channel roughness.
- Develop a potential mass balance that estimates flow volumes when withdrawals and artificial surface returns are removed.

Valid Applications

- Estimate current condition flow volume, velocity and stream depth.
- Estimate potential condition flow volume, velocity and stream depth.
- Identify site specific deviations of current mass balance from the threshold potential mass balance.

Limitations

- Small mass transfer processes are not accounted.
- Limited ground level flow data limit the accuracy of derived mass balances.
- Water withdrawals are not directly quantified
- Water withdrawals are assumed to occur only at OWRD mapped points of diversion.
- Return flows are oversimplified.
- It is not possible to determine the amount of return flows derived from ground water withdrawals relative to those derived from instream withdrawals.
- Return flows may deliver water that is diverted from another watershed.
- Inter-annual variations are not simulated.
- Intra-annual variations are not simulated.

4.1.4 Effective Shade Analysis

Modeling Purpose

- Simulate current condition effective shade levels over stream network.
- Simulate potential condition effective shade levels based on channel width and land cover types and physical attributes over stream network.
- Establish threshold effective shade values for the stream network, below which current conditions are considered to deviate from a potential condition.
- Provide land cover type specific shade curves that allow target development where site-specific targets are not completed.

Valid Applications

- Estimate current condition effective shade over the stream network.
- Estimate potential condition effective shade over the stream network.
- Identify site-specific deviations of current effective shade conditions from threshold potential conditions.

Limitations

- Limitations for input parameters apply (i.e., channel morphology and near stream land cover type and physical attributes).
- Accuracy of the methodology is limited to roughly $\pm$ 8% effective shade.
- The period of simulation is valid for effective shade values that occur in late July and early August.

4.1.5 Stream Temperature Analysis

Modeling Purpose

- Analyze critical condition stream temperature over stream network.
- Analyze potential condition stream temperature based on channel width, land cover types and physical attributes and flow volume over stream network.
- Establish threshold stream temperature values for the stream network, above which current conditions are considered to deviate from a potential condition.
- Demonstrate that stream temperature regimes are significantly different in a condition that minimizes anthropogenic warming.
- Provide a reasonable assurance that beneficial uses are protected in the potential condition to the extent possible given the natural constraints for channel morphology and land cover type and physical attributes.
- Provide a robust methodology for stream temperature analysis, provided data and analytical constraints.

Valid Applications

- Estimate critical condition stream temperatures over the stream network.
- Estimate potential critical condition stream temperatures over the stream network.

- Identify site-specific deviations of current stream temperatures from potential conditions.
- Analyze the sensitivity of single or multiple parameters on stream temperature regimes.
- Identify stream temperature distributions during critical conditions.

Limitations

- Limitations for input parameters apply (i.e., channel morphology, near stream land cover type and physical attributes and hydrology).
- Accuracy of the methodology is limited to validation statistics of results.
- Stream temperature results are limited to the streams for which the analysis is completed (i.e., Nehalem River, North Fork Nehalem River, Cook Creek, Salmonberry River, and Rock Creek). Application of the stream temperature output to other streams within or outside of the North Coast Subbasins is not valid.
- The period of simulation is valid for stream temperature values that occur in late July and early August.
- Inter-annual variations are not simulated.
- Intra-annual variations are not simulated.

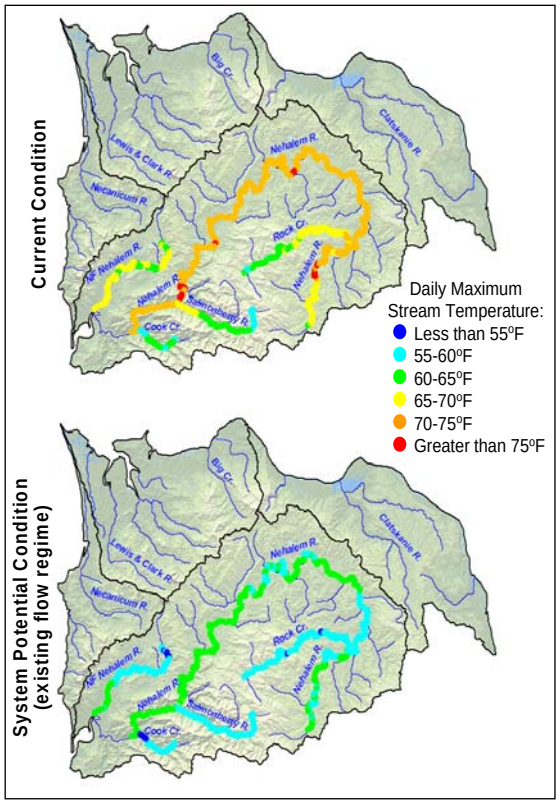

Figure 4-2. *Simulated maximum daily stream temperatures for current conditions and potential channel width, land cover and flow conditions (late July to mid-August period).*

Figure 4-1. *Simulated maximum daily stream temperatures for current conditions and potential channel width, land cover conditions (late July to mid-August period).*

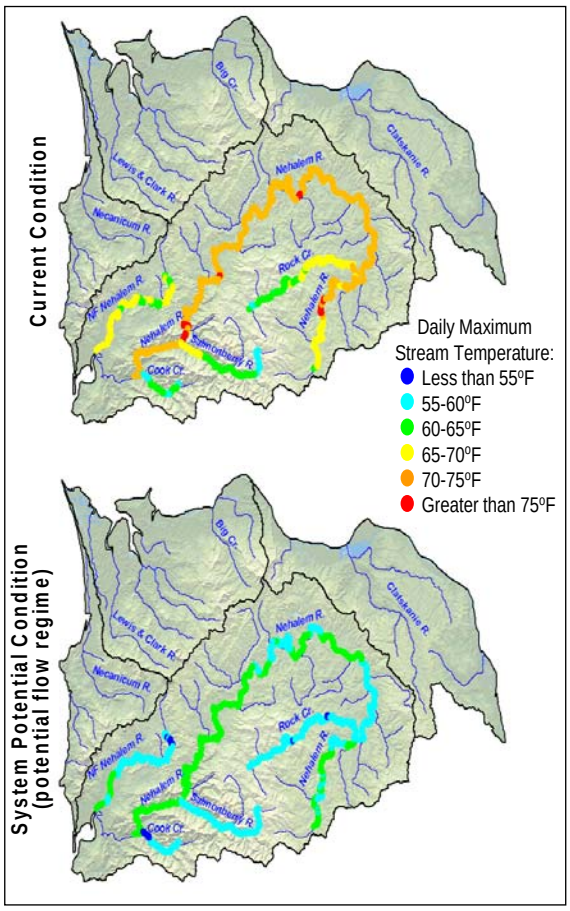

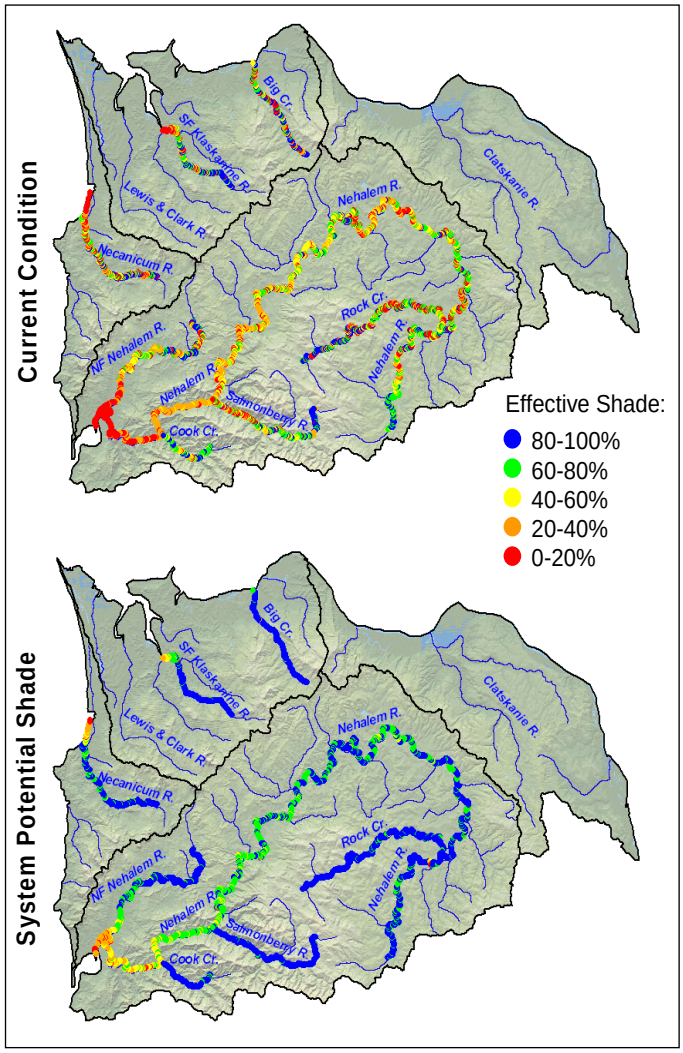

Figure 4-3. *Simulated effective shade – current conditions and potential channel width and land cover conditions (July to August period).*

4.2 EFFECTIVE SHADE

4.2.1 Overview - Description of Shading Processes

Stream surface shade is an important parameter that controls the stream heating derived from solar radiation. Recall that solar radiation has the potential to be the largest heat transfer mechanism in a stream system. Human activities can degrade near stream land cover and/or channel morphology, and in turn, decrease effective shade. It follows that human caused reductions in stream surface shade have the potential to cause significant increases in heat delivery to a stream system. Stream shade levels can also serve as an indicator of near stream land cover and channel morphology condition. For these reasons, stream shade is a focus of this analytical effort.

In the Northern Hemisphere, the earth tilts on its axis toward the sun during summertime months allowing longer day length and higher solar altitude, both of which are functions of solar declination (i.e., a measure of the earth's tilt toward the sun). Geographic position (i.e., latitude and longitude) fixes the stream to a position on the globe, while aspect provides the stream/riparian orientation. Near stream land cover height, width and density describe the physical barriers between the stream and sun that can attenuate and scatter incoming solar radiation (i.e., produce shade). The solar position has a vertical component (i.e., solar altitude) and a horizontal component (i.e., solar azimuth) that are both functions of time/date (i.e., solar declination) and the earth's rotation (i.e., hour angle measured as 15^{o} per hour). While the interaction of these shade variables may seem complex, the mathematics that describes them is relatively straightforward geometry. Using solar tables or mathematical simulations, the *potential daily solar load* can be quantified. The *measured solar load* at the stream surface can easily be measured with a Solar Pathfinder© or estimated using mathematical shade simulation computer programs (Boyd, 1996 and Park, 1993).

Effective Shade Defined

Solar$_1$ – Potential daily direct beam solar radiation load adjusted for julian day, solar altitude, solar azimuth and site elevation.

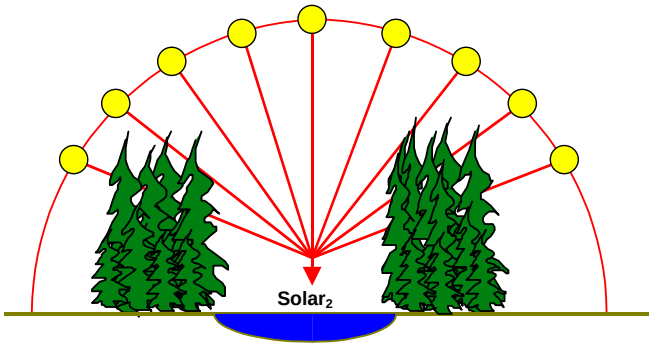

$$\text{Effective Shade} = \frac{(\text{Solar}_1 - \text{Solar}_2)}{\text{Solar}_1}$$

Where,

Solar$_1$: Potential Daily Direct Beam Solar Radiation Load

Solar$_2$: Daily Direct Beam Solar Radiation Load Received at the Stream Surface

Figure 4-4. *Definition of effective shade*

Geometric Relationship that Influence Shade Production

Solar Altitude and **Solar Azimuth** are two basic measurements of the sun's position. When a stream's orientation, geographic position, riparian condition and solar position are known, shading characteristics can be simulated.

Solar Altitude measures the vertical component of the sun's position
Solar Azimuth measures the horizontal component of the sun's position

Figure 4-5. *Parameters that affect shade and geometric relationships*

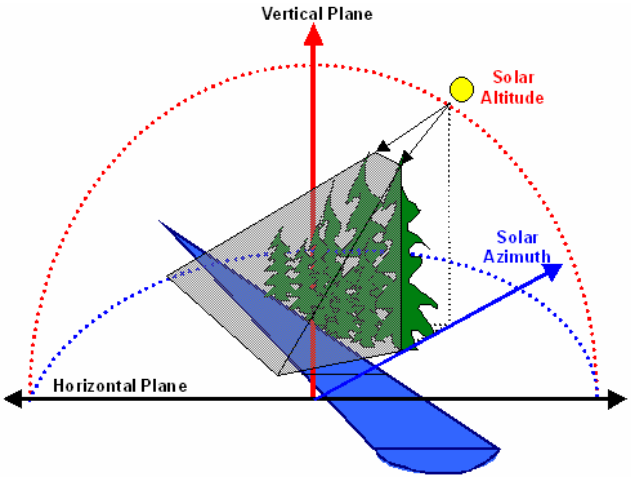

Table 4-1. Factors that Influence Stream Surface Shade

***Blue* – Not Influenced by Human Activities**
***Red* - Influenced by Human Activities**

Description	***Parameter***
Season/Time	Date/Time
Stream Characteristics	Aspect, Channel Width
Geographic Position	Latitude, Longitude
Vegetative Characteristics	Near Stream Land cover Height, Width, Density
Solar Position	Solar Altitude, Solar Azimuth

4.2.2 Effective Shade Simulation Methodology

Using computer software developed by DEQ[1], stream surface shade can be simulated at a landscape scale. Topographic shade angle, channel morphology and land cover derived spatial data sets serve as high resolution input data. Stream surface shade production is a function of geometric relationships between the sun's position and topography, near stream land cover and channel features. For any given location, the sun's position is a function of time (i.e., season and time of day). Provided an accurate location description (i.e., latitude and longitude), the exact position of the sun for any given time can be easily simulated.

A vector between the sun and the stream can then be calculated. Topographic, land cover and/or stream channel features that obstruct the sun → stream vector create shade. Shade produced by topographic features and/or channel banks completely attenuates direct beam solar radiation. The shading algorithms mimic the travel direction of a photon from the sun to the stream. The first potential barrier to a photon is a topographic feature. If the sun angle is greater than that of topographic features, then the stream is not shaded from surrounding topography. The direct beam is then routed to the top of the land cover boundaries.

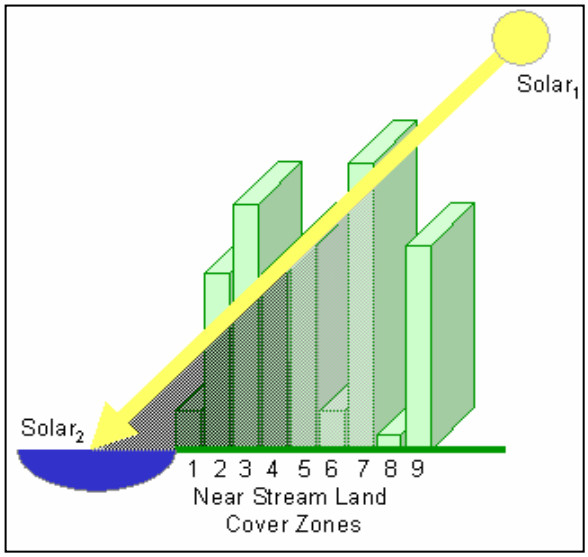

Land cover is broken into nine consecutive zones, each is fifteen feet in width, and located in the transverse direction. The direct beam is routed through the vegetation zones, staring at the outer zone 9. Each land cover height is checked to see if it intersects the sun → stream vector. If it does, then the attenuation of direct beam solar radiation caused by the land cover zone occurs as a function of a light extinction coefficient and the path length through the land cover zone. Path length through the land cover zone is a function of zone width, stream aspect, solar altitude and solar azimuth. Attenuation is calculated using Beer's Law (Oke, 1978). Direct beam radiant energy that passes through a land cover zone is then routed to the next inner land cover zone and the process is repeated. Once through all nine land cover zones, remaining direct beam solar radiation is routed to the stream surface. Diffuse solar radiation filters through the canopy and is attenuated as a function of canopy opening. If only the portion of the stream surface is shaded, while the remaining portion is exposed to direct beam solar radiation, the land cover attenuated solar flux is used for the shaded portion, and an unattenuated solar flux is used for the non-shaded portion. At the stream surface, the remaining direct beam and the received diffuse solar radiation are summed and become the solar load received at the top of the stream surface ($Solar_2$).

A portion of solar radiation is reflected off the stream surface as a function of the solar angle, while the remaining portion enters the water column. The water column solar path length is a function of the solar angle and water depth. The portion of the received direct beam solar radiation absorbed by the water column is a function of water column path length and the transmissivity of the water column. The remaining solar radiation is received at the stream bed, where a portion is absorbed as a function of solar angle and literature values for reflectivity properties of quartz (Beschta and Weatherred, 1984). Heat absorbed by the streambed will cause differential heating and start conducting back to the water column. The remaining portion of solar direct beam radiation is reflected off the stream bed and travels towards

[1] DEQ has developed and maintains a computer application called Shade-a-lator that can predict stream surface shade at a user defined spatial scales.

the surface of the stream, where again there is absorption of remain solar radiation in the water column as a function of path length and stream transmissivity.

Below are the steps used for calculating effective shade. Effective shade is a ratio of the received solar load to the total potential solar load. Both total potential and received solar radiation is calculated for any given day at a 10-minute time step for each stream data node.

1. Calculate solar position as a function of time and in relation to a defined location. Variables calculated are:
   - solar altitude
   - solar zenith
   - solar declination
   - solar azimuth

2. Calculate direct beam and diffuse beam solar radiation received at the top of the land cover boundary. Variables calculated are:
   - air mass thickness
   - air mass transmissivity
   - topographic shade angle
   - solar load received at edge of atmosphere
   - direct beam solar radiation received at top of land cover boundary
   - diffuse solar radiation received at top of land cover boundary
   - potential solar load

3. Calculate direct beam and diffuse beam solar radiation received at the top of the stream surface. Direct beam solar radiation is routed through all land cover zones (i.e., 9 zones every 15 feet starting at the furthest from the stream channel). Diffuse solar radiation is proportional to the canopy opening. Variables calculated are:
   - percent canopy opening
   - land cover transmissivity
   - path length through land cover
   - direct beam solar radiation received at top of stream
   - diffuse solar radiation received at top of stream
   - shadow extension into the stream channel
   - portion of the stream channel shaded (0 to 1)
   - total solar load received at top of stream

4. Calculate solar radiation absorbed in the water column and streambed. Variables calculated are:
   - water surface reflectivity
   - water column transmissivity
   - streambed reflectivity
   - path length through water column
   - total solar load received by water column

5. Calculate effective shade. Variables calculated are:

- $Solar_1$ = daily sum of potential solar load
- $Solar_2$ = daily sum of total solar load received at top of water column
- Effective Shade = ($Solar_1$ - $Solar_2$) / $Solar_1$

4.2.2.1 Effective Shade Simulation Period and Extent

The effective shade analysis was conducted with data input sampling and a computation rate every 100 feet along stream segments. The effective shade model is calibrated to analyze and predict stream temperature for narrow periods of time as a function of Julian Day, however other periods can be simulated. Periods of simulation occurred in early to mid August and output data is reliable for the July through August period. Effective shade simulations were performed for a total of 229.6 river miles in the Nehalem, Necanicum, and Lower Columbia River subbasins. **Table 4-2** lists the spatial extent and simulation period for by river system.

Table 4-2. Effective Shade Simulation Periods and Extent

Subbasin	River/Stream	Simulation Extent
Nehalem River Subbasin	Nehalem River	RM 0.7 to 111.1
	Rock Creek	RM 0 to 25.9
	Salmonberry River	RM 0 to RM 16
	North Fork Salmonberry River	RM 0 to 8.9
	Cook Creek	RM 0 to 6.7
	North Fork Nehalem River	RM 0 to 20.2
Necanicum River Subbasin	Necanicum River	RM 0 to 16.7
Lower Columbia Subbasin	Klaskanine River	RM 0 to 2.8
	South Fork Klaskanine River	RM 0 to 9.8
	Big Creek	RM 0 to 12.2
		Total Simulation Extent 229.6 river miles

4.2.2.2 Simulated Effective Shade Scenarios

Once effective shade models are calibrated, potential channel width and land cover scenarios are simulated. The combinations of potential channel width and near stream land cover are simulated together to maximize the benefits of potential land cover physical properties and channel width reductions related to shade production.

Shade Scenario 1: Current Condition

Shade Scenario 2: Potential Channel Width
Potential Near Stream Land Cover
All other inputs remain unchanged

4.2.2.2 Validation - Effective Shade Simulation Accuracy

Effective shade simulation validation was conducted by comparing simulated results with ground level measured effective shade values. Solar Pathfinder® data was used to collect all ground level data at 20 different locations. Shade simulations have a standard error of 7.8% when compared to these values. The correlation coefficient between measured and simulated values is high (i.e., $R^2 = 0.92$). The statistical significance of model output is roughly 8% effective shade. **Figure 4-6** shows the simulated effective shade values plotted against the measured effective shade values.

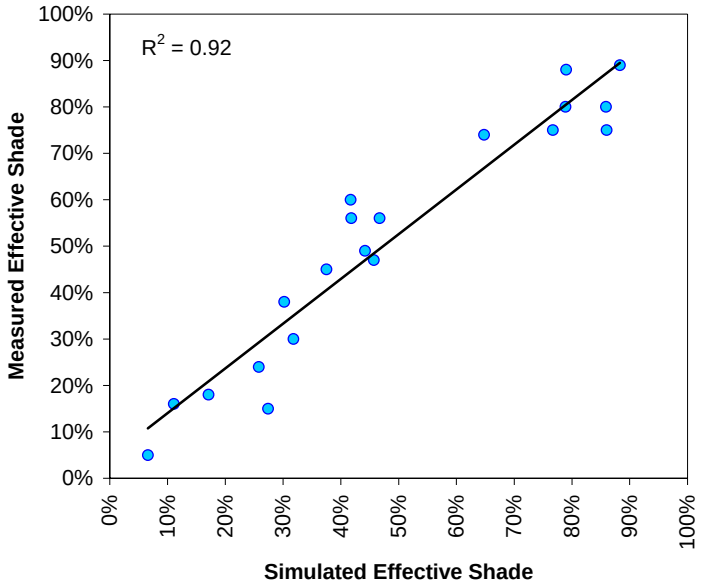

Figure 4-6. *Simulated effective shade compared to ground level measured effective shade.*

4.2.3 Effective Shade and Solar Heat Flux Simulations

4.2.3.1 Site Specific Effective Shade Simulations

Figure 4-7. *Simulated effective shade data - Current condition and Potential Condition.*

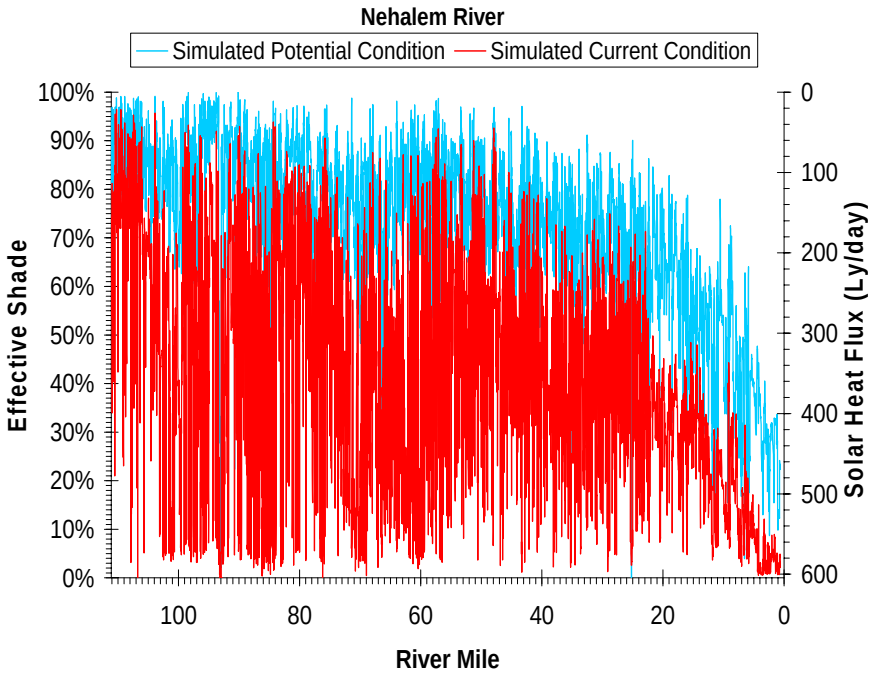

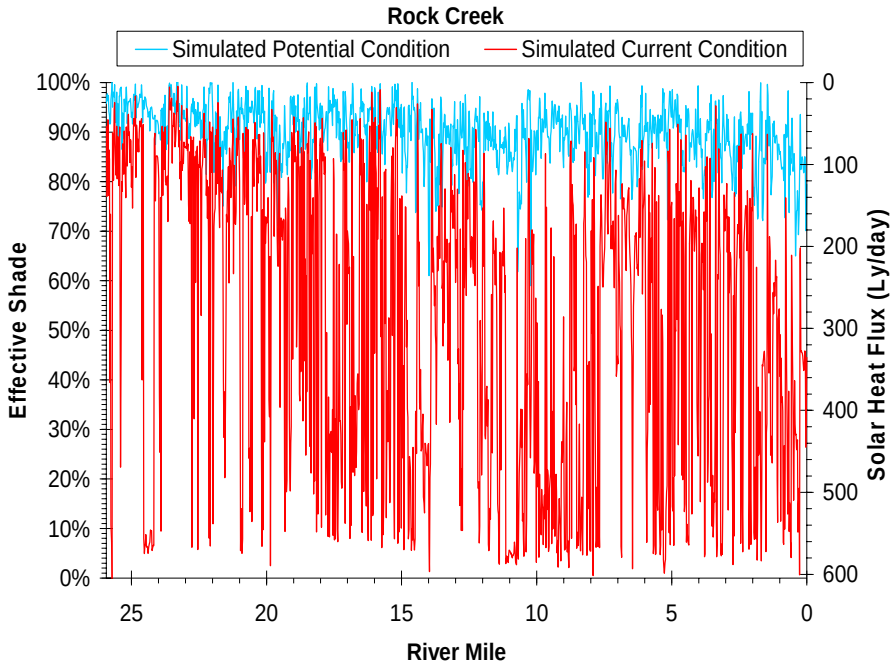
Rock Creek
Simulated Potential Condition
Simulated Current Condition
Effective Shade
100%
90%
80%
70%
60%
50%
40%
30%
20%
10%
0%
Solar Heat Flux (Ly/day)
0
100
200
300
400
500
600
25
20
15
10
5
0
River Mile

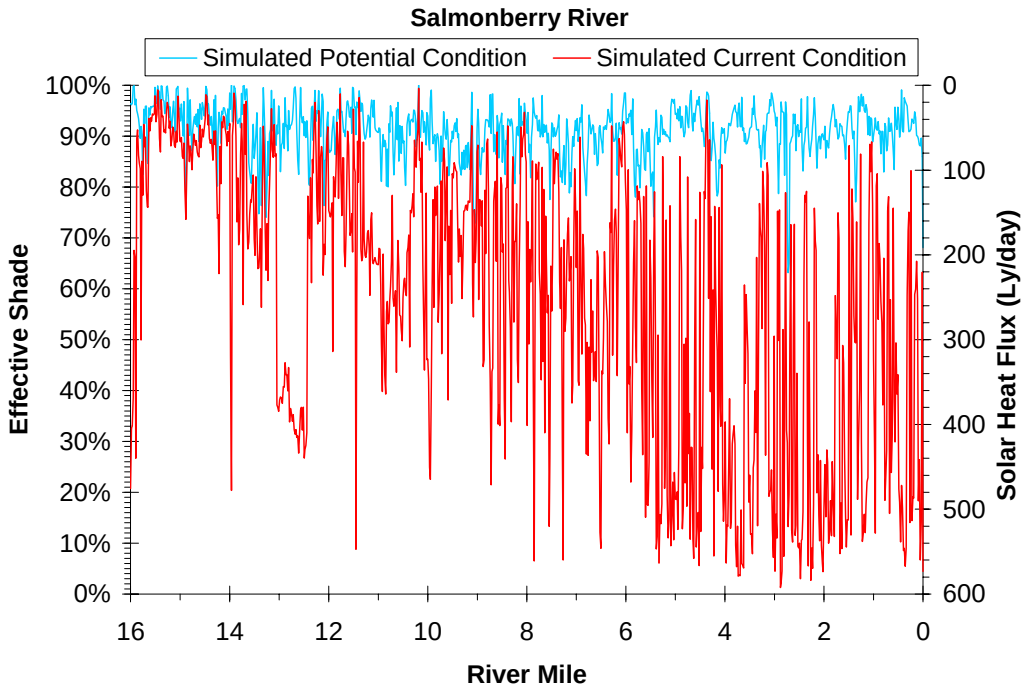
Salmonberry River
Simulated Potential Condition
Simulated Current Condition
Effective Shade
100%
90%
80%
70%
60%
50%
40%
30%
20%
10%
0%
Solar Heat Flux (Ly/day)
0
100
200
300
400
500
600
16
14
12
10
8
6
4
2
0
River Mile

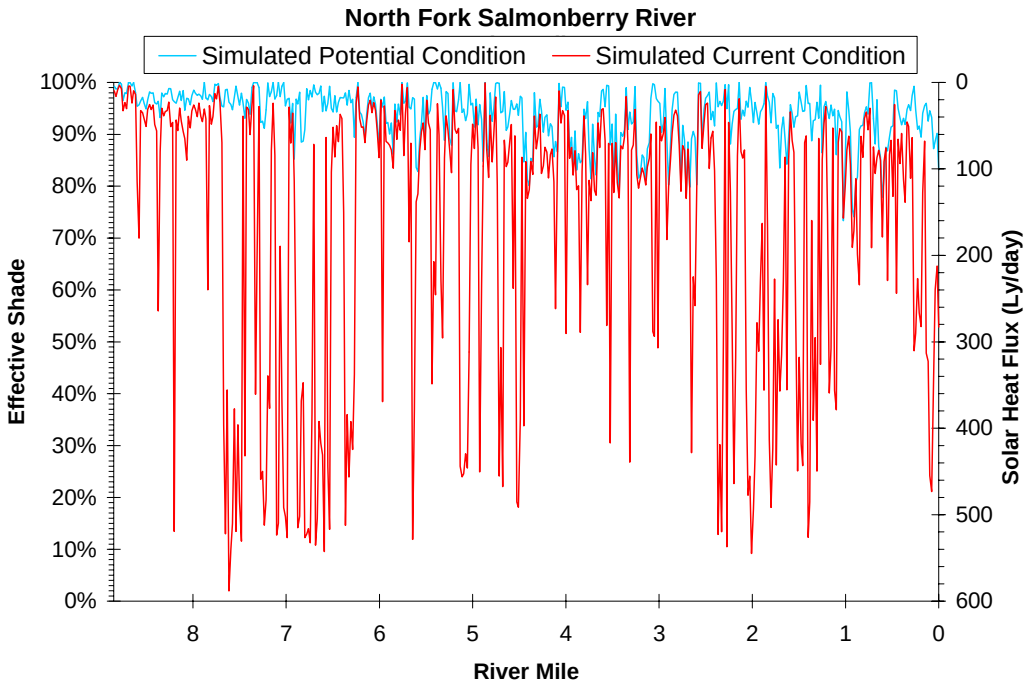

Figure 4-7 (continued). *Simulated effective shade data - Current condition and Potential Condition.*

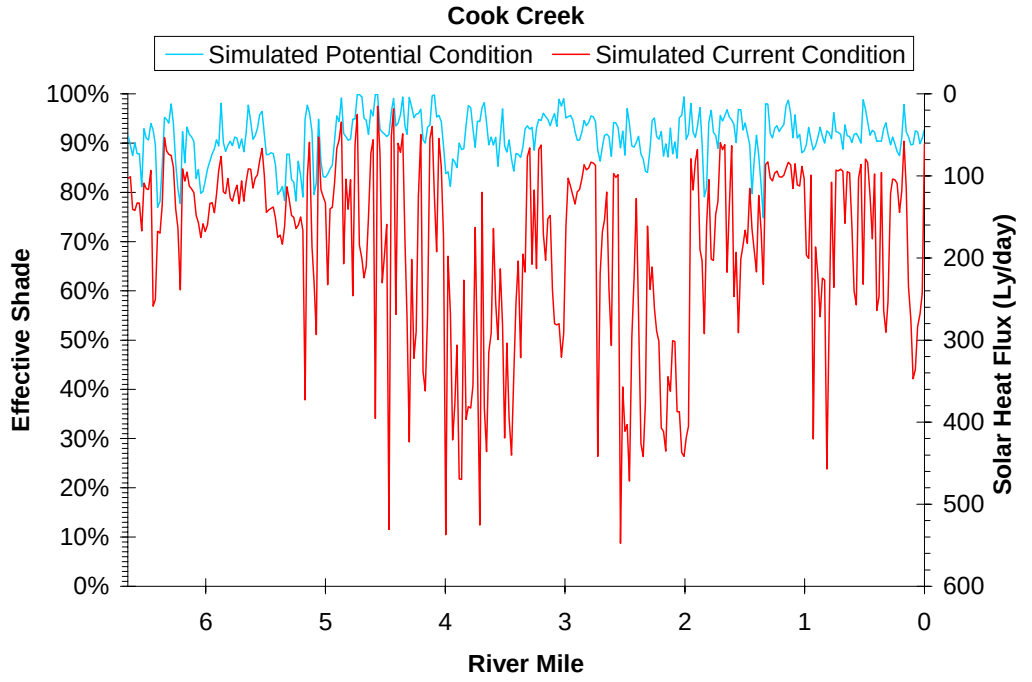

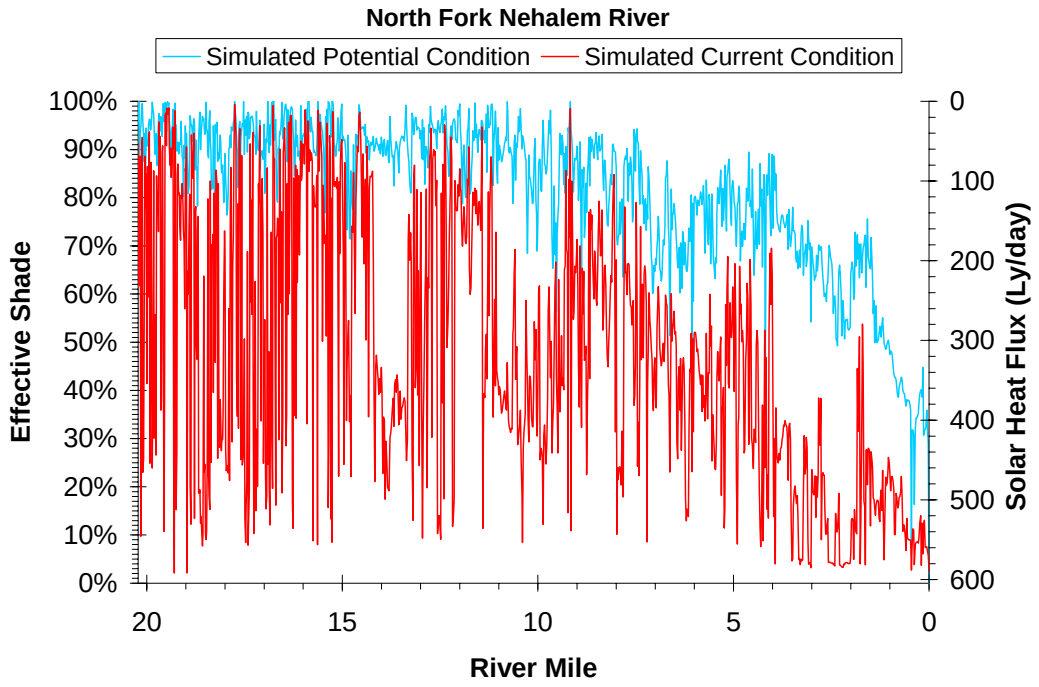

Figure 4-7 (continued). *Simulated effective shade data - Current condition and Potential Condition.*

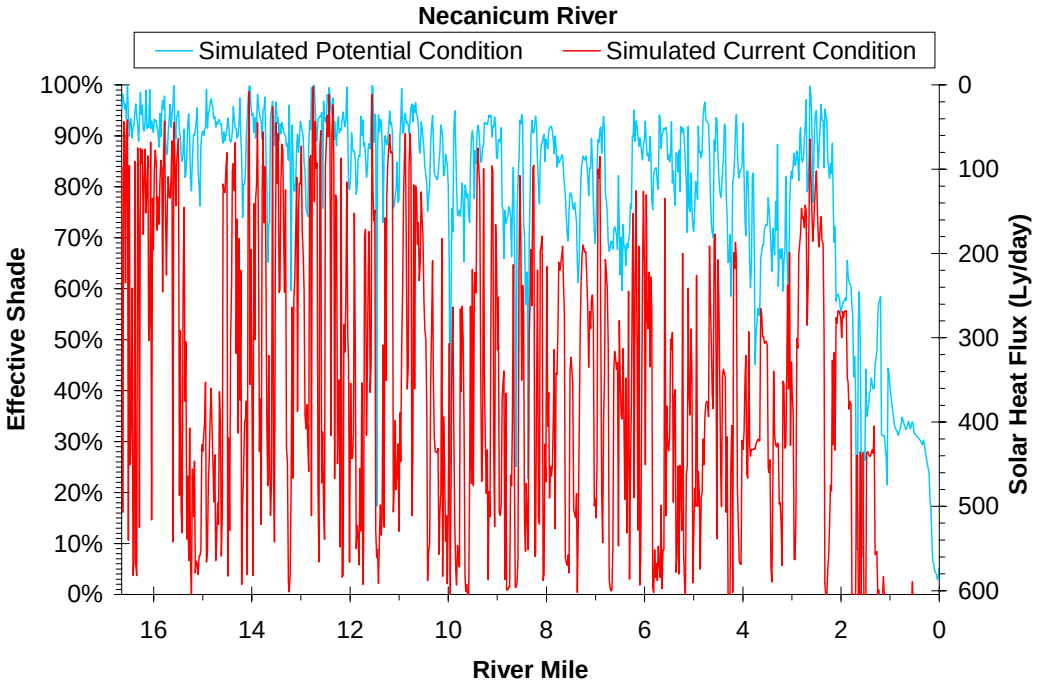

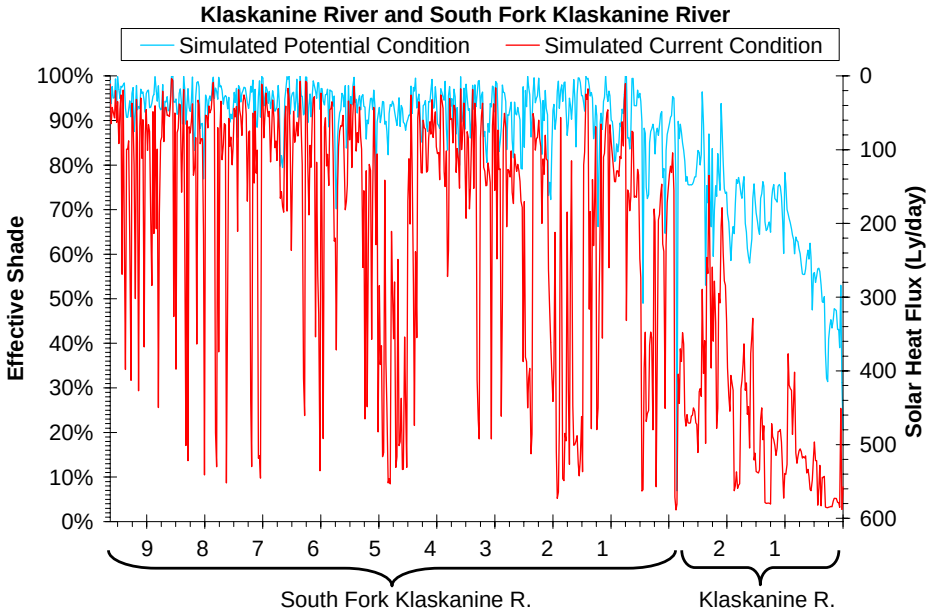

Figure 4-7 (continued). *Simulated effective shade data - Current condition and Potential Condition.*

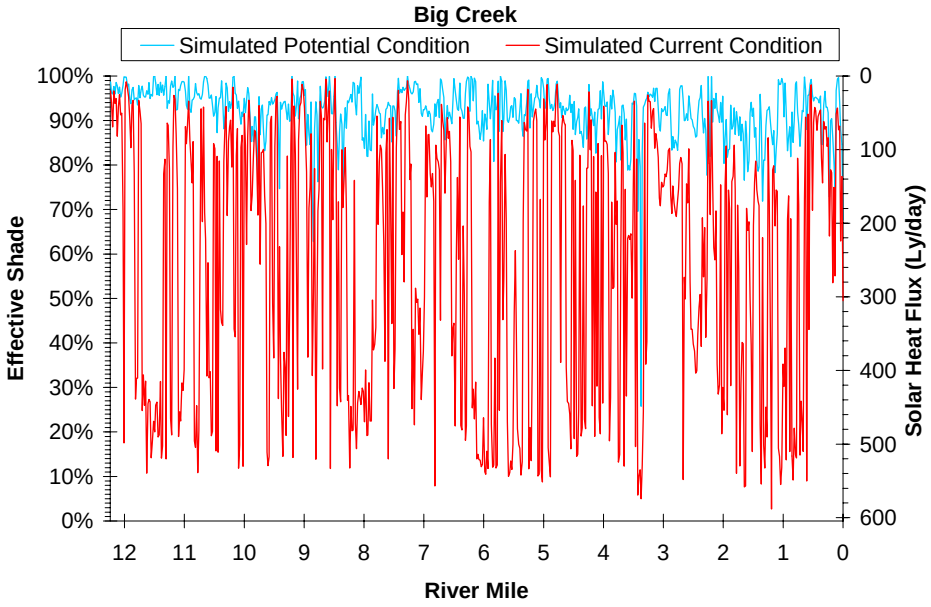

Figure 4-7 (continued). *Simulated Effective Shade Data - Current Condition and Potential Condition.*

For the sake of comparison, average effective shade values are presented in **Figure 4-8**. Several observations can be made from the simulations results. Effective shade levels are generally moderate to good in the North Coast Subbasins, in both the current and system potential conditions. Increases in stream shade will directly reduce solar radiation and reduce both daily maximum stream temperatures and daily fluctuation of stream temperature. This holds true when shade levels are increased from any level. So even minor increases in shade will reduce the heat transfer to the stream system.

Another observation is that lower river reaches have less shade than upper reaches. This is mainly the result of larger channel widths. Large channels combined with shorter land cover (i.e., deciduous hardwoods often dominate lower elevation flood plains near the stream) limits the amount of shade received. The opposite is also observed in the average shade data. Higher shade levels occur in upper reaches with narrower channels and that generally have taller growing land cover types.

Figure 4-8. *Average simulated effective shade data - Current condition and System potential condition.*

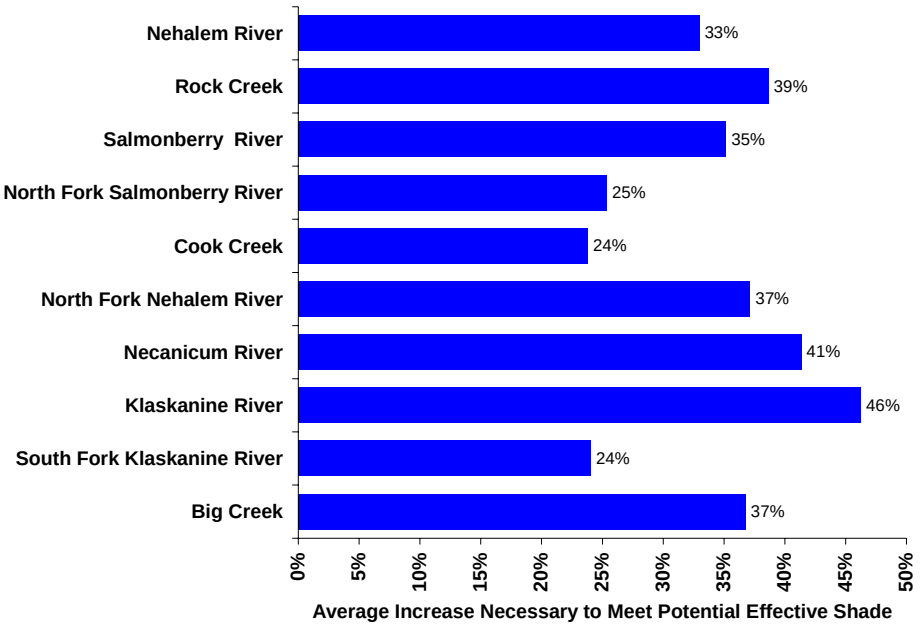

Figure 4-9.

The percent increase in effective shade levels from the current condition to the System potential condition.

4.2.4 Total Daily Solar Heat Load Analysis

Solar heating is established as a primary pollutant in stream heating processes. The calculation of the overall heat load received by the stream system from solar radiation yields the nonpoint sources of solar heat for the total stream system as well as for each stream/river. The total daily solar heat load is the cumulative solar heat received by a stream over one day during the critical period (i.e., July/August period). For the purposes of this analytical effort, the total solar heat load is the sum of the products of the daily solar heat flux and surface area of exposure for each stream reach (i.e., for each stream data node every 100 ft).

$$H_{solar} = \sum \left(\Phi_{solar} \cdot A_y \right) = \sum \left(\Phi_{solar} \cdot W_{wetted} \cdot dx \right)$$

Background levels of solar heat estimate the portion of the total daily solar heat load that occurs when nonpoint sources of heat are minimized. The background condition is the system potential total daily solar heat load (i.e., where anthropogenic nonpoint sources are minimized) and is calculated by substituting the system potential daily solar flux and the potential wetted width into the equation above. In this fashion, the total daily solar load is calculated for both the current condition (H_{solar}) and the system potential condition ($H_{solar}^{Background}$). With the background portion of the total daily solar load accounted for, the remaining portion can be attributed to anthropogenic nonpoint sources. Therefore, the anthropogenic nonpoint source total daily solar load is the difference between the total daily solar load and the background total daily solar load. Derived total daily solar loads for background sources and anthropogenic nonpoint sources are presented in **Figure 4-10**.

$$H_{solar}^{NPS} = H_{solar} - H_{solar}^{Background}$$

where,

A_y: Stream surface area unique to each stream segment (cm^2)

Dx: Stream segment length and distance step in the methodology (cm)

Φ_{solar}: Solar heat flux for unique to each stream segment (kcal cm^{-2} day^{-1})

H_{solar}: Total daily solar heat load delivered to the stream (kcal day^{-1})

H_{solar}^{NPS}: Portion of the total daily solar heat load delivered to the stream that originates from nonpoint sources of pollution (kcal day^{-1})

$H_{solar}^{Background}$: Portion of the total daily solar heat load delivered to the stream that originates from background sources of pollution that are not affected by human activities (kcal day^{-1})

W_{wetted}: Wetted width unique to each stream segment (cm)

Roughly one half of the solar loading that occurs in the North Coast Subbasins stream systems, including major tributaries, is from anthropogenic nonpoint sources, while the remaining one half of the total daily solar load originates from background sources (see **Figure 4-11**). *For the purposes of this analysis the total heat load is calculated from the simulated current condition. The background condition is calculated from the System potential channel width and land cover condition simulation. The nonpoint source load is the difference between the current total daily solar load and the background total daily solar heat load.*

Figure 4-12 displays the solar heat load contributions for each stream simulated. The Nehalem River appears to have the most solar heat load, largely due to the fact that it is a longer and wider river than the other streams that it is being compared to. In any case, anthropogenic nonpoint sources account for about half of the solar heat load in most streams simulated.

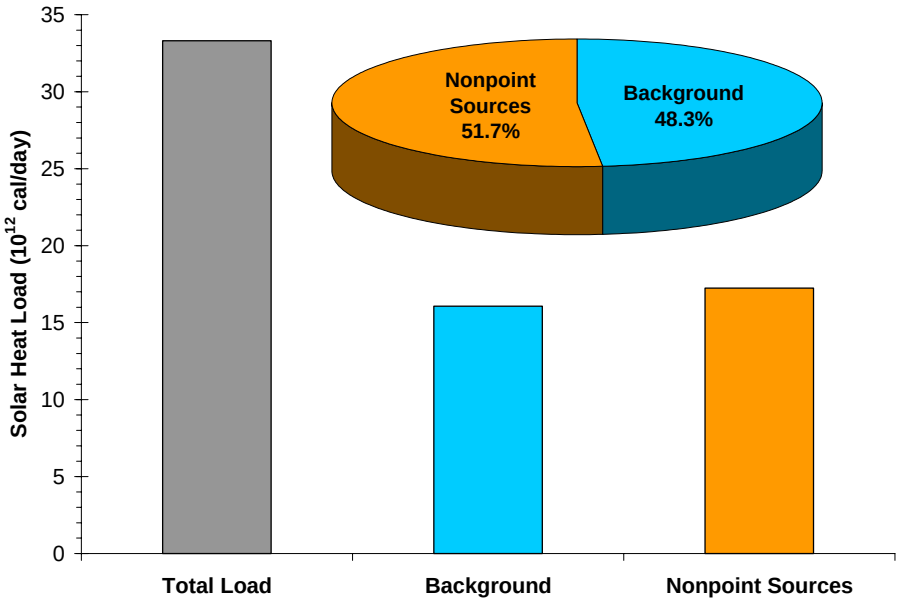

Figure 4-10. *Total daily solar heat load derived as the sum of the products of the daily solar heat flux and channel surface area.*

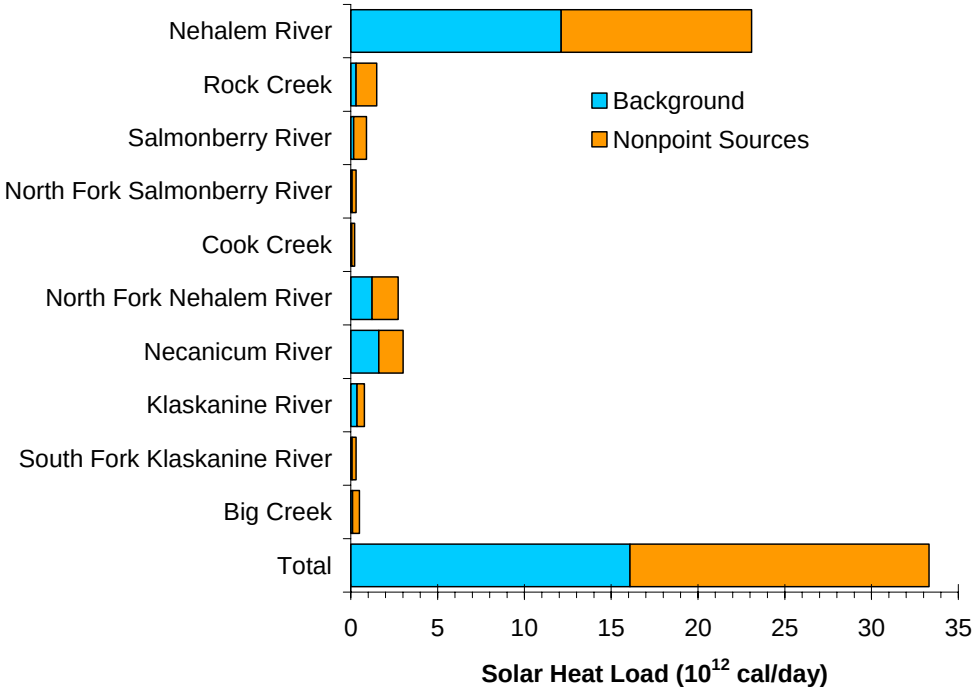

Figure 4-11. *Distribution of the total solar heat load for anthropogenic nonpoint sources and background sources by stream/river system.*

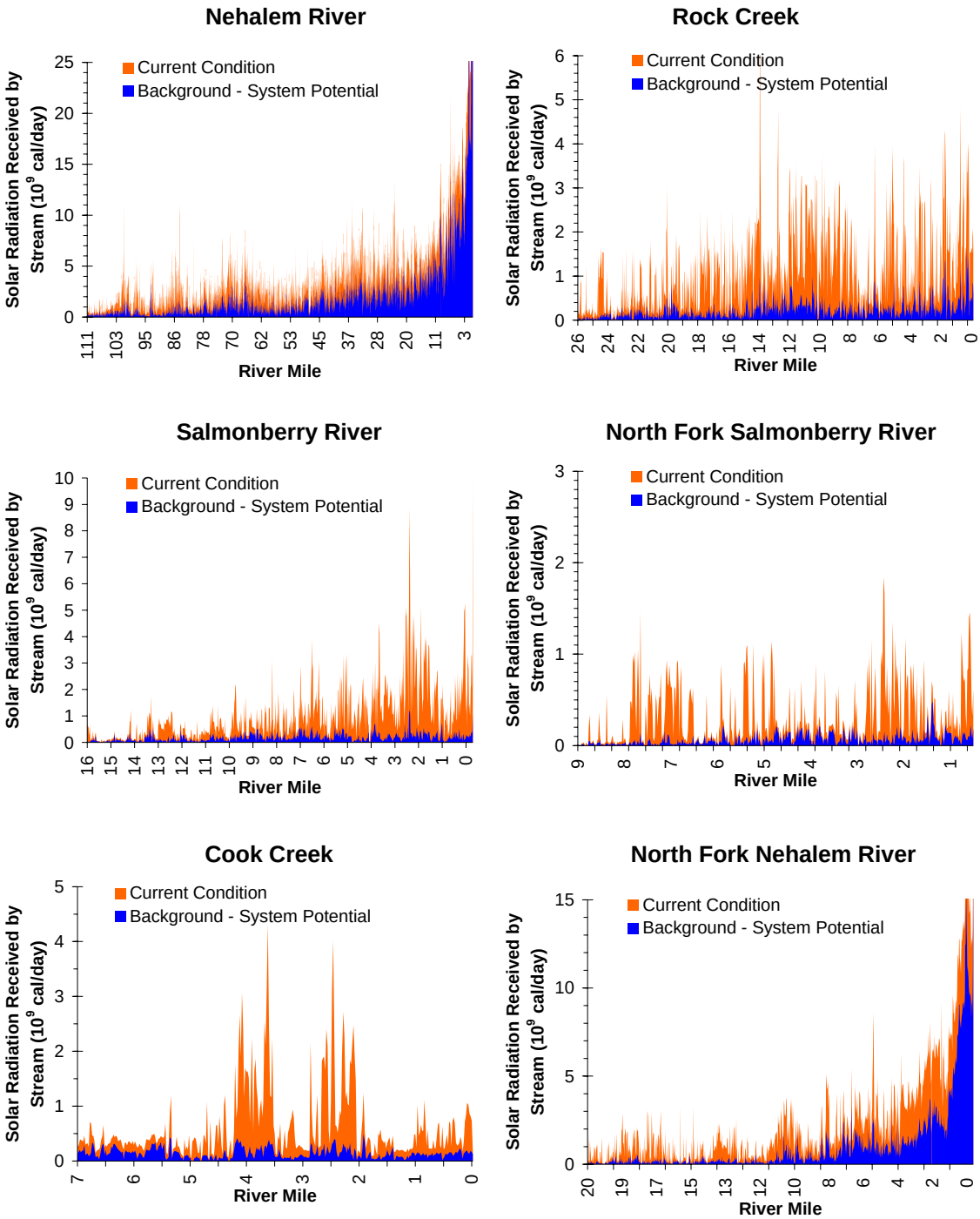

Figure 4-12. *Total daily solar heat loads derived from solar heat flux and channel surface area.*

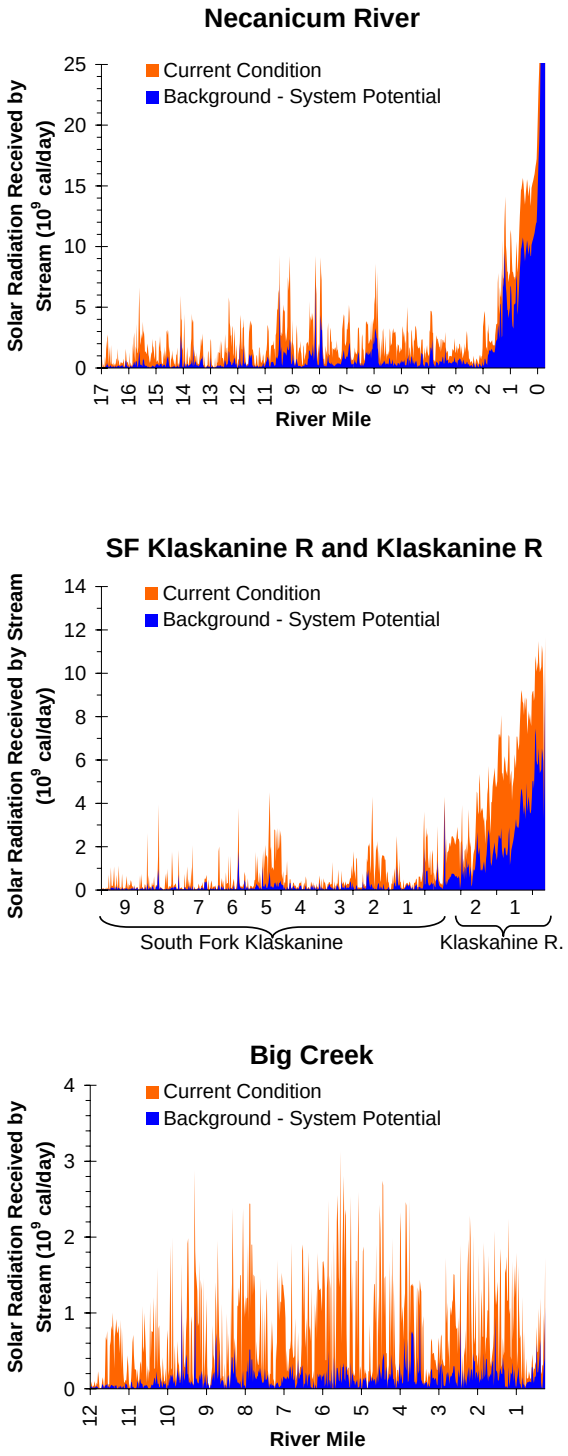

Figure 4-12 (continued). *Total daily solar heat loads derived from solar heat flux and channel surface area.*

4.2.5 Effective Shade Curve Development

Effective shade curves are designed to display effective shade levels for a specific land cover type as a function of channel width. These shade curves are intended to provide effective shade targets where site-specific effective shade simulations have not been completed. For a list of stream segments where effective shade simulations have been performed reference **Section 4.2.2.1 Effective Shade Simulation Period and Extent.** Effective shade curves presented in this document are developed for the North Coast Subbasins (i.e. latitude and longitude) and are accurate for the critical time period (i.e. July/August). Stream aspect is also considered in the shade curve methodology.

Figure 1.
The land cover types used for development of the shade curves are those developed as the potential land cover types: large conifer, large hardwood, and large conifer/hardwood mix. For more information regarding the potential land cover types reference **Section 3.5.3 Near Stream Land Cover - Potential Condition Development.** Land cover physical dimensions for height and density are listed on the shade curves. Determination of appropriate potential land cover types is the responsibility of the designated management agencies and private citizens.

Channel width targets can be determined from Rosgen channel type and drainage area regressions developed in **Section 3.4.4 Channel Width Assessment.** Recall that potential channel width is a function of potential Rosgen stream type and drainage area. Determination of the appropriate potential Rosgen stream type is the responsibility of the designated management agencies and private citizens.

Figures 4-13 to **4-15** display shade curves for the potential land cover types. This methodology provides land cover, channel width and effective shade targets for the remaining portions of the North Coast Subbasins. The shade curves also demonstrate the relationship between land cover physical properties, channel width and stream aspect.

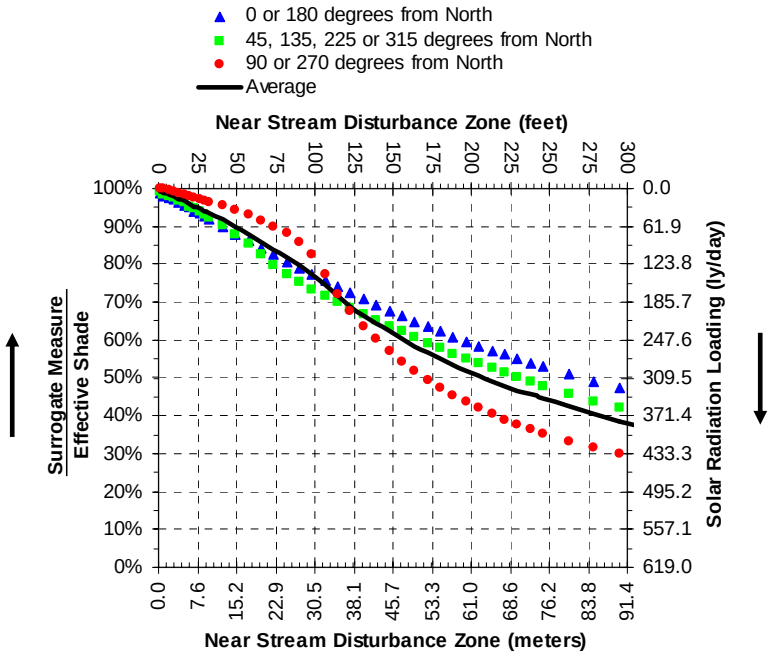

Figure 4-13. *Effective shade curves for the conifer land cover type - 175 feet tall and 90% density.*

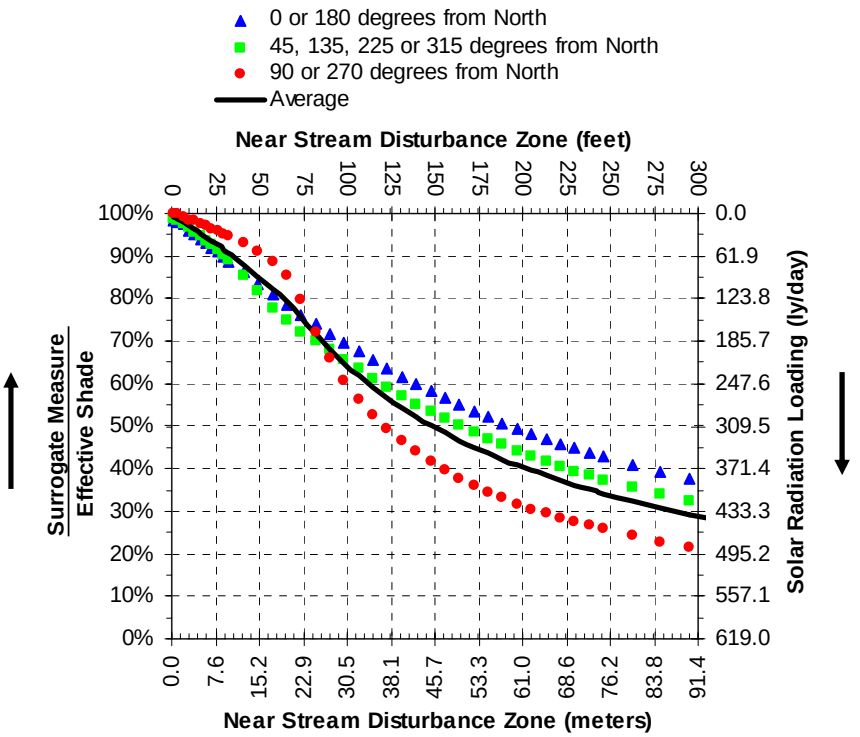

Figure 4-14. *Effective shade curves for the deciduous/conifer mix land cover type – 125 feet tall and 90% density.*

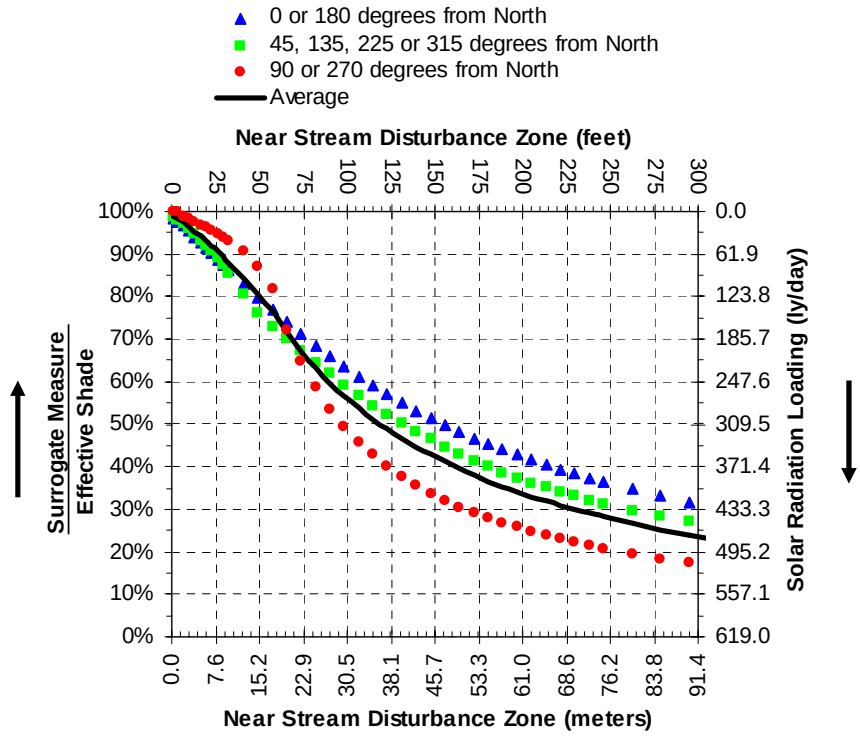

Figure 4-15. *Effective shade curves for the deciduous land cover type – 100 feet tall and 90% density.*

4.3 STREAM TEMPERATURE SIMULATIONS

4.3.1 Stream Temperature Simulation Methodology

Water temperature change is a function of the heat transfer in a discrete volume. Similarly, heat is a measure of stream temperature change, based on the properties of water. By excluding constants, it can be demonstrated that temperature change is proportional to heat and inversely proportional to river flow rates.

Calculation of Heat,

$$H = \Delta T_R \cdot M_R \cdot c_w = \Delta T_R \cdot (Q_R \cdot t \cdot \rho_w) \cdot c_w$$

Calculation of Water Temperature Change,

$$\Delta T_R = \frac{H}{M_R \cdot c_w} = \frac{H}{(Q_R \cdot t \cdot \rho_w) \cdot c_w}$$

Excluding constants, water temperature change is a function of heat and river flow,

$$\Delta T_R \propto H, \ \frac{1}{Q_R}$$

where,

Metric units are used in all computations

ΔT_R : Change in river temperature (^oC)

H : Heat (cal)

Q_R : Flow rate (cms)

M_R : Mass of river volume (kg)

c_w : Specific heat of water $\left(10^3 \frac{cal}{kg} = \frac{kcal}{kg}\right)$

ρ_w : Density of water $\left(10^3 \frac{kg}{m^3}\right)$

t : Duration (sec)

All heat transfer rates can be quantified as a flux, which implies heat transfer per a unit area per a unit time. For computational purposes this methodology relies on heat flux metric units.

$$\text{Heat Flux} = \frac{\text{Heat}}{\text{Area} \cdot \text{Time}} = \frac{cal}{cm^2 \cdot sec} = \frac{ly}{sec}$$

Water has a relatively high heat capacity ($c_w = 10^3$ cal kg^{-1} K^{-1}) (Satterlund and Adams 1992). Conceptually, water is a heat sink. Heat that is gained by the stream is retained and only slowly released back to the surrounding environment. Heat released from the stream to the surrounding environment is represented by a negative heat flux ($\Phi_{cooling}$). Heat delivered to the stream is a positive heat flux ($\Phi_{heating}$). Excluding mass transfer processes, heating periods occur when the net heat flux (Φ_{total}) is positive. Cooling periods occur when the net heat flux is negative.

$$\Phi_{total} = \Phi_{heating} + \Phi_{cooling}$$

4.3.1.1 Heat Transfer Processes

In general, the net heat flux experienced by all stream/river systems follows two cycles: a seasonal cycle and a diurnal cycle. In the Pacific Northwest, the seasonal net heat cycle experiences a maximum

positive flux during summer months (July and August), while the minimum seasonal flux occurs in winter months (December and January). The diurnal net heat cycle experiences a daily maximum flux that occurs at or near the sun's zenith angle, while the daily minimum flux often occurs during the late night or the early morning. It should be noted, however, that meteorological conditions are variable. Cloud cover and precipitation seriously alter the heat relationships between the stream and its environment.

The ultimate source of heat to a stream system is solar radiation both diffuse and direct. Secondary sources of heat include longwave radiation (also referred to as thermal radiation) from the atmosphere and streamside vegetation, streambed conduction, and in some cases, groundwater exchange at the water-stream bed interface. Several processes dissipate heat at the air-water interface, namely: evaporation, convection and back radiation. Heat is acquired by the stream system when the flux of heat energy entering the stream is greater than the flux of heat energy leaving. The net heat flux provides the rate at which energy is gained or lost per unit area and is represented as the instantaneous summation of all heat energy components. The net heat flux (Φ_{total}) consists of several individual thermodynamic heat flux components, namely: solar radiation (Φ_{solar}), long-wave radiation ($\Phi_{longwave}$), conduction ($\Phi_{conduction}$), groundwater exchange ($\Phi_{groundwater}$) and evaporation ($\Phi_{evaporation}$) (Wunderlich, 1972; Jobson and Keefer, 1979; Beschta and Weatherred, 1984; Sinokrot and Stefan, 1993; Boyd, 1996). With the exception of solar radiation, which only delivers heat energy, these processes are capable of both introducing and removing heat from a stream. The instantaneous heat transfer rate experienced by the stream is the summation of the individual processes.

When a stream surface is exposed to midday solar radiation, large quantities of heat will be delivered to the stream system (Brown 1969, Beschta et al. 1987). Some of the incoming solar radiation will reflect off the stream surface, depending on the elevation of the sun. All solar radiation outside the visible spectrum (0.36μ to 0.76μ) is absorbed in the first meter below the stream surface and only visible light penetrates to greater depths (Wunderlich, 1972). Sellers (1965) reported that 50% of solar energy passing through the stream surface is absorbed in the first 10 cm of the water column. Removal of riparian vegetation, and the shade it provides, contributes to elevated stream temperatures (Rishel et al., 1982; Brown, 1983; Beschta et al., 1987). The principal source of heat energy delivered to the water column is solar energy striking the stream surface directly (Brown 1970). Exposure to direct solar radiation will often cause a dramatic increase in stream temperatures. The ability of riparian vegetation to shade the stream throughout the day depends on land cover height, width, density and position relative to the stream (i.e. stream aspect). *Solar Radiation* (Φ_{Solar}) is a function of the solar angle, solar azimuth, solar declination, atmospheric properties, topography, location and near stream land cover. Simulation is based on methodologies developed by Ibqal (1983), Beschta and Weatherred (1984), Chen (1996) and Boyd (1996).

Both the atmosphere and vegetation along stream banks emit longwave radiation that can heat the stream surface. Water is nearly opaque to longwave radiation and complete absorption of all wavelengths greater than 1.2μ occurs in the first 5 cm (i.e. less than 2 inches) below the surface (Wunderlich, 1972). Longwave radiation has a cooling influence when emitted from the stream surface. The net transfer of heat via longwave radiation usually balances so that the amount of heat entering is similar to the rate of heat leaving the stream (Beschta and Weatherred, 1984; Boyd, 1996). Warm stream temperatures often cause the longwave radiation balance to become negative and the net longwave heat exchange from the atmosphere, near stream land cover and stream surface has a cooling effect (Boyd, 1996). *Longwave Radiation* ($\Phi_{Longwave}$) is derived by the Stefan-Boltzmann Law and is a function of the emissivity of the body, the Stefan-Boltzmann constant and the temperature of the body (Wunderlich, 1972)

Evaporation occurs in response to internal energy of the stream (molecular motion) that randomly expels water molecules from the stream surface into the overlying air mass. Evaporation is the most effective method of dissipating heat from water (Parker and Krenkel, 1969). As stream temperatures increase, so does the rate of evaporation. Air movement (wind) and low vapor pressures increase the rate of evaporation and accelerate stream cooling (Harbeck and Meyers, 1970). *Evaporation* ($\Phi_{Evaporation}$) relies

on a Dalton-type equation that utilizes an exchange coefficient, the latent heat of vaporization, wind speed, saturation vapor pressure and vapor pressure (Wunderlich, 1972).

Convection transfers heat between the stream and the air via molecular and turbulent conduction (Beschta and Weatherred, 1984). Heat is transferred in the direction of warmer to cooler. Air can have a warming influence on the stream when the stream is cooler. The opposite is also true. The amount of convective heat transfer between the stream and air is low (Parker and Krenkel, 1969; Brown, 1983, Beschta and Weatherred, 1984). Nevertheless, air temperatures play a role in stream temperature dynamics via convection, as well as, secondary effects to other heat transfer processes affected by vapor pressure and atmospheric thermal radiation. All of these processes are accounted for in the simulation methodology. *Convection* ($\Phi_{Convection}$) is a function of the Bowen Ratio and terms include atmospheric pressure, and water and air temperatures.

Depending on streambed composition, shallow streams (less than 20 cm) may allow solar radiation to warm the streambed (Brown, 1969). Large cobble (> 25 cm diameter) dominated streambeds in shallow streams may store and conduct heat as long as the bed is warmer than the stream. Bed conduction may cause maximum stream temperatures to occur later in the day, possibly into the evening hours. *Bed Conduction* ($\Phi_{Conduction}$) simulates the theoretical relationship ($\Phi_{Conduction} = K \cdot dT_b / dz$), where calculations are a function of thermal conductivity of the bed (K) and the temperature gradient of the bed (dT_b/dz) (Sinokrot and Stefan, 1993). Bed conduction is solved with empirical equations developed by Beschta and Weatherred (1984).

Net Heat Flux Continuity Equation,

$$\Phi_{Total} = \Phi_{Solar} + \Phi_{Longwave} + \Phi_{Evaporation} + \Phi_{Convection} + \Phi_{Conduction}.$$

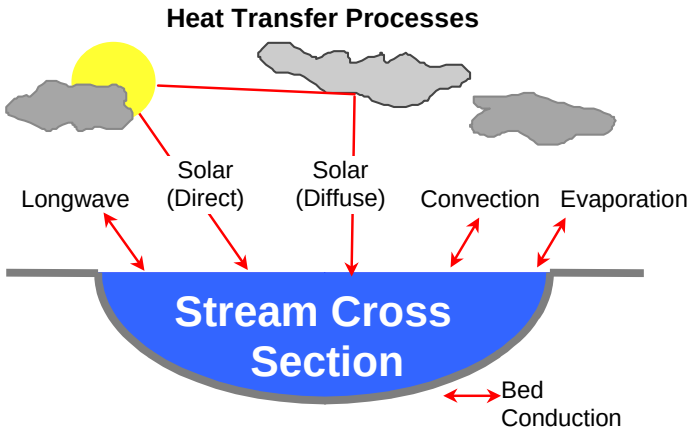

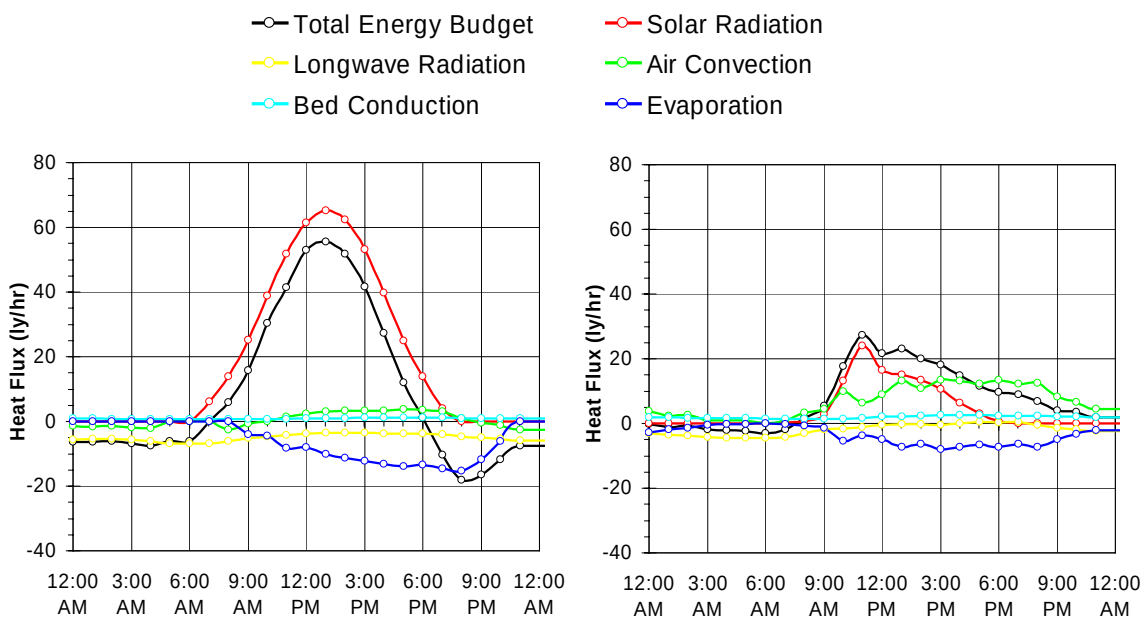

Figure 4-16. *Examples of simulated heat transfer processes. These heat transfer outputs are generated at every distance node in the model methodology.*

The rate change in stream temperature is driven by the heat energy flux (Φ_i). It is easily shown that a defined volume of water will attain a predictable rate change in temperature, provided an accurate prediction of the heat energy flux. The rate change in stream temperature (T) is calculated as a function of wetted channel heat flux, wetted depth and several constants.

Rate Change in Temperature Caused by Heat Energy Thermodynamics,

$$\frac{\partial T}{\partial t} = \left(\frac{Ax_i \cdot \Phi_i}{\rho \cdot c_p \cdot V_i} \right),$$

Which reduces to,

$$\frac{\partial T}{\partial t} = \left(\frac{\Phi_i}{\rho \cdot c_p \cdot D_i} \right).$$

Where,

Ax_i: cross-sectional area (m^2)
C_p: specific heat of water (cal $kg^{-1} \cdot {}^oC^{-1}$)
D_i: average stream depth (m)
t: time (s)
T: Temperature (^oC)
V_i: Volume (m^3)
Φ_i: total heat energy flux (cal $m^{-2} \cdot s^{-1}$)
ρ: density of water (1000 kg/m^3)

4.3.1.2 Mass Transfer Processes

Stream flow velocity (U_x) is calculated using Manning's equation as a function of the channel hydraulic radius (R_h), stream gradient (S_o) and channel roughness estimates (n). The hydraulic radius is the ratio of the cross-sectional area (A_x) to the wetted perimeter (P_w). Channel shape is assumed to be rectangular.

Under this assumption, the wetted cross-sectional area is the product of average depth (D) and wetted width (W). The wetted perimeter is the sum of the two wetted channel sides and the wetted width ($2 \cdot D + W$). Stream gradient data is derived from digital elevation model data and stream segment length information from digitized stream polylines (see **Section 3.4.3**). Wetted width data is sampled from digitized channel polylines from aerial photos. Simulation inputs for channel roughness values are within the literature values for Rosgen level I stream types.

$$U_x = \frac{1}{n} \cdot S_o^{1/2} \cdot R_h^{2/3} = \frac{1}{n} \cdot S_o^{1/2} \cdot \left(\frac{A_x}{P_w} \right)^{2/3} = \frac{1}{n} \cdot S_o^{1/2} \cdot \left(\frac{D \cdot W}{2 \cdot D + W} \right)^{2/3}$$

Advection redistributes heat energy in the positive longitudinal direction. No heat energy is lost or gained by the system during advection, and instead, heat energy is transferred downstream as a function of flow velocity. In the case where flow is uniform, the rate change in temperature due to advection is expressed in the first order partial differential equation below.

Rate Change in Temperature Caused by Advection,

$$\frac{\partial T}{\partial t} = -U_x \cdot \frac{\partial T}{\partial x}$$

Dispersion processes occur in both the upstream and downstream direction along the longitudinal axis. Heat energy contained in the system is conserved throughout dispersion, and similar to advection, heat energy is simply moved throughout the system. The rate change in temperature due to dispersion is expressed in the second order partial differential equation below.

Rate Change in Temperature Caused by Dispersion,

$$\frac{\partial T}{\partial t} = D_L \cdot \frac{\partial^2 T}{\partial x^2}$$

The dispersion coefficient (D_L) may be calculated by stream dimensions, roughness and flow. In streams that exhibit high flow velocities and low longitudinal temperature gradients, it may be assumed that the system is advection dominated and the dispersion coefficient may be set to zero (Sinokrot and Stefan 1993). In the event that dispersion effects are considered significant, the appropriate value for the dispersion coefficient can be estimated with a practical approach developed and employed in the QUAL 2e model (Brown and Barnwell 1987). An advantage to this approach is that each parameter is easily measured, or in the case of Manning's coefficient (n) and the dispersion constant (K_d), estimated.

Physical Dispersion Coefficient,

$$D_L = C \cdot K_d \cdot n \cdot U_x \cdot D^{\frac{5}{6}}$$

The simultaneous non-uniform one-dimensional transfer of heat energy is the summation of the rate change in temperature due to heat energy thermodynamics, advection and dispersion. Given that the stream is subject to steady flow conditions and is well mixed, transverse temperature gradients are negligible (Sinokrot and Stefan 1993). An assumption of non-uniform flow implies that cross-sectional area and flow velocity vary with respect to longitudinal position. The following second ordered parabolic partial differential equation describes the rate change in temperature for non-uniform flow.

Non-Uniform One-dimensional Heat Energy Transfer,

$$\frac{\partial T}{\partial t} = -U_x \cdot \frac{\partial T}{\partial x} + D_L \cdot \frac{\partial^2 T}{\partial x^2} + \frac{\Phi}{c_p \cdot \rho \cdot D}$$

$$\text{Steady Flow: } \frac{\partial U_x}{\partial t} = 0$$

$$\text{Non-Uniform Flow: } \frac{\partial U_x}{\partial x} \neq 0$$

Where,

A_x: Cross-Sectional area of wetted channel (m^2)
C: Unit conversion
C = 3.82 for English units
C = 1.00 for Metric units
c_p: **Figure 2.** **Specific heat of water (10^3 cal kg^{-1} K^{-1})**
D: Average stream depth (m)
D_L: Dispersion coefficient (m^2/s)
Φ: **Figure 3.** **Heat flux (cal $m^{-2}s$)**
K_d: Dispersion constant
N: Manning's coefficient
P_w: Wetted perimeter (m)
R_h: Hydraulic radius (m)
ρ: Density of water (10^3 kg m^{-3})
S_o: Stream gradient
U_x: Average flow velocity (m/s)
W: Wetted width (m)

The solution to the *one-dimensional heat energy transfer equation* is essentially the summation of thermodynamic heat energy exchange between the stream system and the surrounding environment and physical processes that redistribute heat energy within the stream system. It is important to note that all heat energy introduced into the stream is conserved, with the net heat energy value reflected as stream temperature magnitude. Further, heat energy is transient within the stream system, due to longitudinal transfer of heat energy (i.e., advection and dispersion). The net heat energy flux (Φ) is calculated at every distance step and time step based on physical and empirical formulations developed for each significant energy component. The dispersion coefficient (D_L) is assumed to equal zero.

4.3.1.3 Boundary Conditions and Initial Values

The temperatures at the upstream boundary (i_o) for all time steps (t_o ,t_1,..., t_{M-1}, t_M) are supplied by the upstream temperature inputs. At the downstream boundary temperature at longitudinal position i_{n+1} is assumed to equals that of i_n with respect to time t. Initial values of the temperatures at each distance node (i_o ,i_1,..., i_{N-1}, i_N) occurring at the starting time (t_o) can be input by the model user or assumed to equal the boundary condition at time t_o.

4.3.1.4 Simulated Scenarios

Once stream temperature models are calibrated, several scenarios are simulated by changing one or more stream input parameters. The simulated scenarios focus largely on defined potential conditions for channel width, land cover and derived flow mass balances. Combinations of these potential conditions are also simulated to investigate the cumulative thermal effect of attaining defined conditions. These scenarios are also used for sensitivity analysis.

Scenario 1: Current Condition
Scenario 2: Potential Near Stream Disturbance Zone (NSDZ) Width
All other inputs remain unchanged
Scenario 3: Potential Near Stream Land Cover
All other inputs remain unchanged
Scenario 4: Potential Flow
All other inputs remain unchanged
Scenario 5: Tributaries Less than 64°F
All other inputs remain unchanged
Scenario 6: Tributaries Less than 64°F
Potential Near Stream Disturbance Zone (NSDZ) Width
Potential Near Stream Land Cover
Scenario 7: Tributaries Less than 64°F
Potential Near Stream Disturbance Zone (NSDZ) Width
Potential Near Stream Land Cover
Potential Flow

4.3.1.5 Spatial and Temporal Scale

The lengths of the defined finite difference and data input sampling rate is 100 feet. The temperature model is calibrated to analyze and predict stream temperature for one day, however multiple days can be simulated. Prediction time steps are limited by stability considerations for the finite difference solution method. Periods of simulation occurred in early August. Simulations were performed for a total of 163.1 WRD river miles in the Nehalem River subbasin. **Table 4-3** lists the spatial extent and simulation period for by river system.

Table 4-3. Stream Temperature Simulation Periods and Extent

River/Stream	Simulation Period	Simulation Extent
Rock Creek	August 6, 2000	RM 25.9 to 0
Salmonberry River	August 4, 2000	RM 16.0 to 0
Cook Creek	August 6, 2000	RM 6.7 to 0
North Fork Nehalem River	August 8, 2000	RM 20.2 to 4.8
Nehalem River	August 5, 2000	RM 111.1 to 12.0
		Total Simulation Extent 163.1 WRD river miles

4.3.1.6 Validation - Simulation Accuracy

For the purposes of this analytical effort, validation refers to the statistical comparison of measured and simulated data. Absolute average deviation and standard error statistics are calculated for FLIR derived spatial temperature data sets, instream measured temporal temperature data sets and combined spatial and temporal data sets. Each measurement of temperature is discrete and is used to assess model accuracy. Simulation outputs are only accurate to levels that exceed the validation statistics. A statistically significant simulated result is one that produces a temperature change greater than validation statistics listed in **Table 4-4**.

Stream temperatures derived from FLIR data offer an extremely robust validation data set for spatial stream temperature simulation tools. Since the FLIR temperature data is continuous, the number of simulated temperatures available for model validation is limited to model resolution. With FLIR temperature data, the spatial scalability for any given methodology is unlimited by validation data. This

represents a significant improvement over previous data sources. As an example, DEQ simulated stream temperatures for the Salmonberry River along 16 river miles. The selected model spatial resolution was 100 meters, allowing 274 discrete model output samples for calculation of validation statistics. A similar effort that relied simply on available instream continuous monitors would have allowed only 72 validation samples.

Spatial and temporal data is stratified in the validation to test for biases in the simulation methodology. Since FLIR temperature data sets are robust spatially, there is a possibility that the simulation could be calibrated to the specific time when FLIR data was obtained, yet perform poorly for other periods of the day. However, validation statistics demonstrate that this is not the case. The overall simulation performance is validated using 3,199 discrete measurements and simulations of stream temperatures during the simulation period. The absolute average deviation from measured data is 1.5^{o}F and the standard error in 0.6^{o}F. **Figure 4-17** displays the validation results for each simulated stream and river in the Nehalem River subbasin.

Table 4-4. Stream Temperature Simulation Validation

	Validation Statistic	Nehalem River	Rock Creek	Salmon-berry River	Cook Creek	North Fork Nehalem River
Temporal Instream Data	Samples (n)	264	48	72	72	48
	Ave. Deviation (°F)	1.6	4.1	1.5	2.5	1.5
	Standard Error (°F)	0.84	1.08	0.48	0.74	0.68
Spatial FLIR Derived Temperature	Samples (n)	1,636	419	274	107	259
	Ave. Deviation (°F)	1.27	0.74	0.68	0.44	0.83
	Standard Error (°F)	1.56	0.20	0.12	0.07	0.12

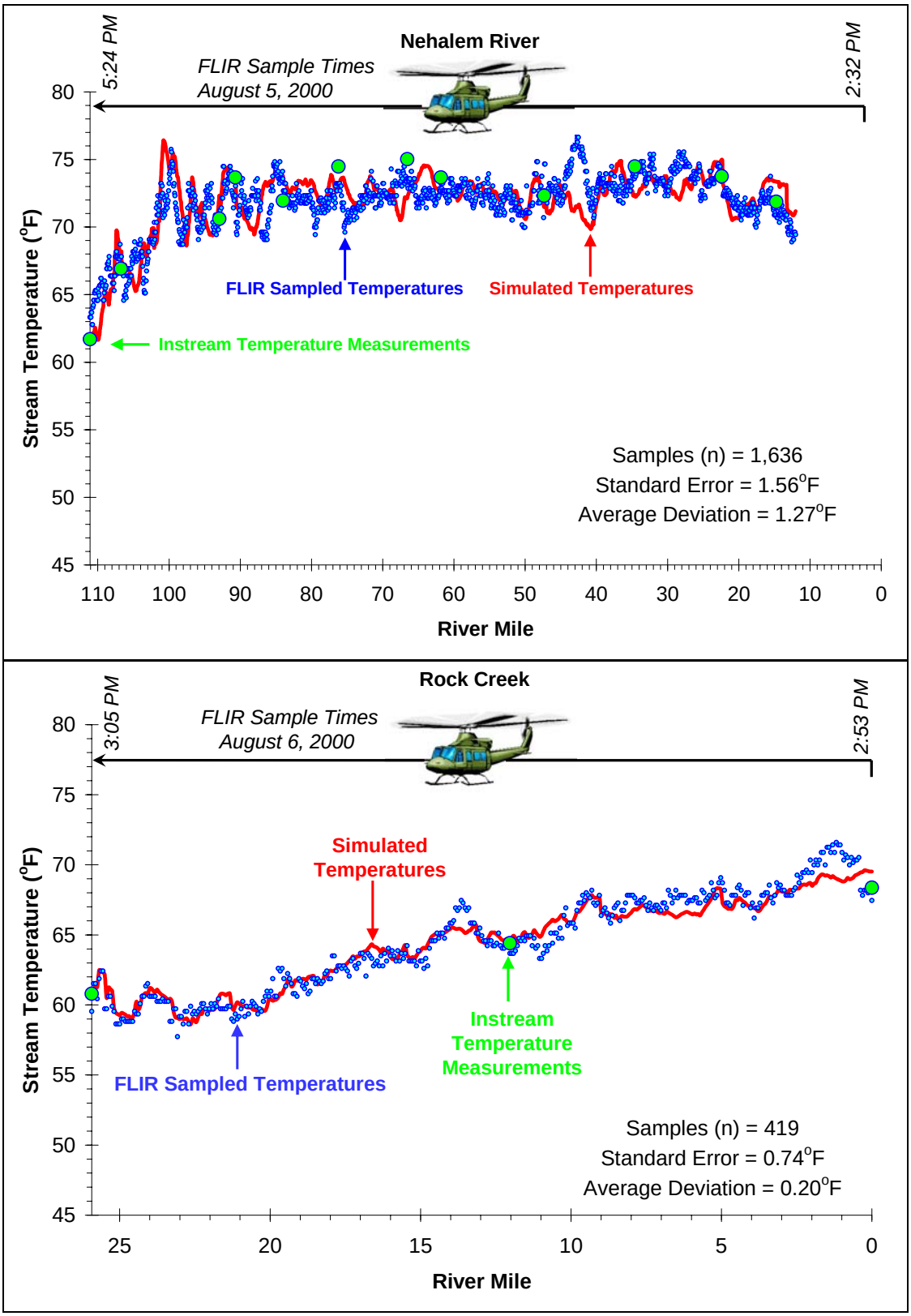

Figure 4-17. *Stream Temperature Simulation Compared to FLIR Derived Stream Temperatures*

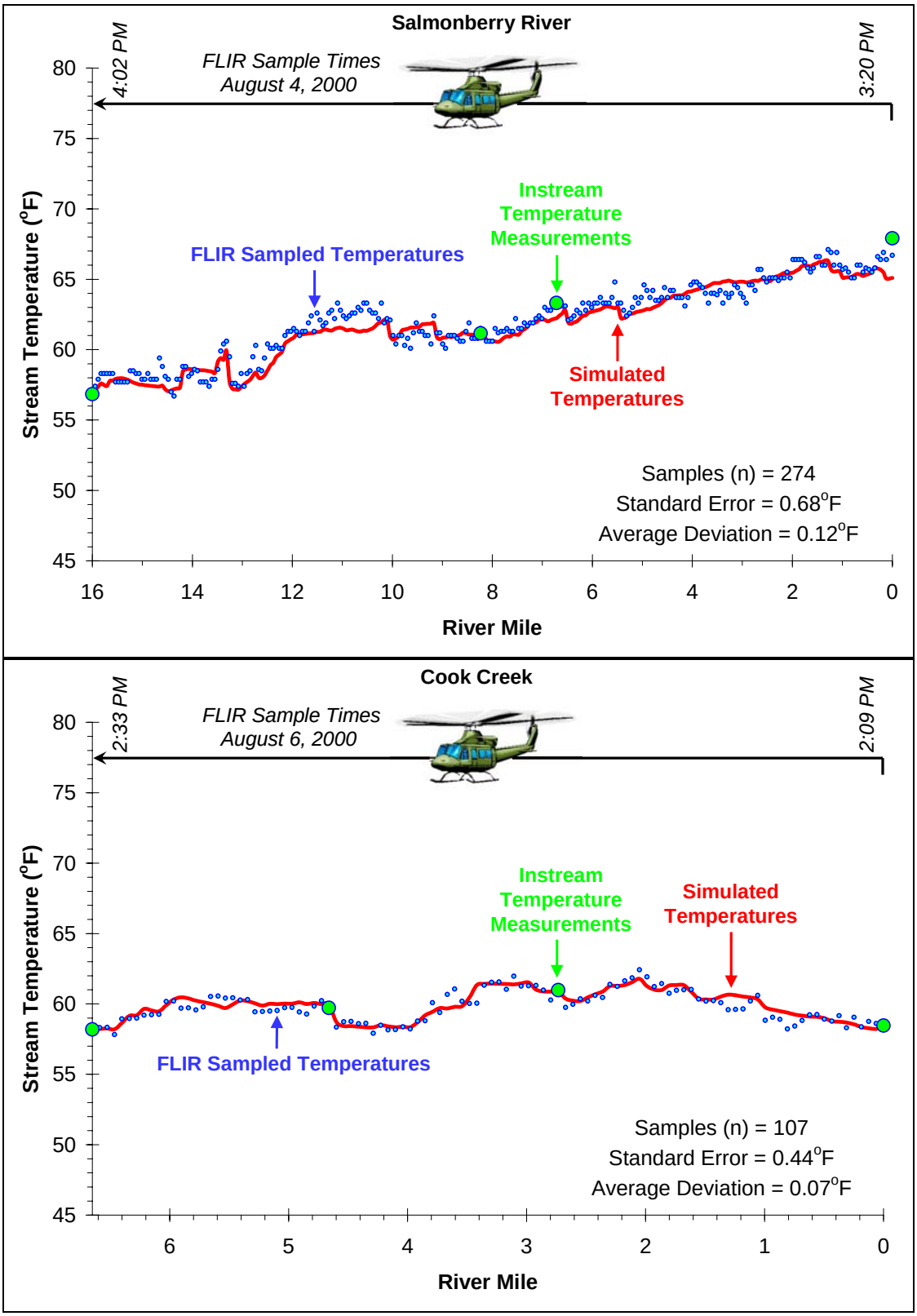

Figure 4-17 (continued). *Stream Temperature Simulation Compared to FLIR Derived Stream Temperatures*

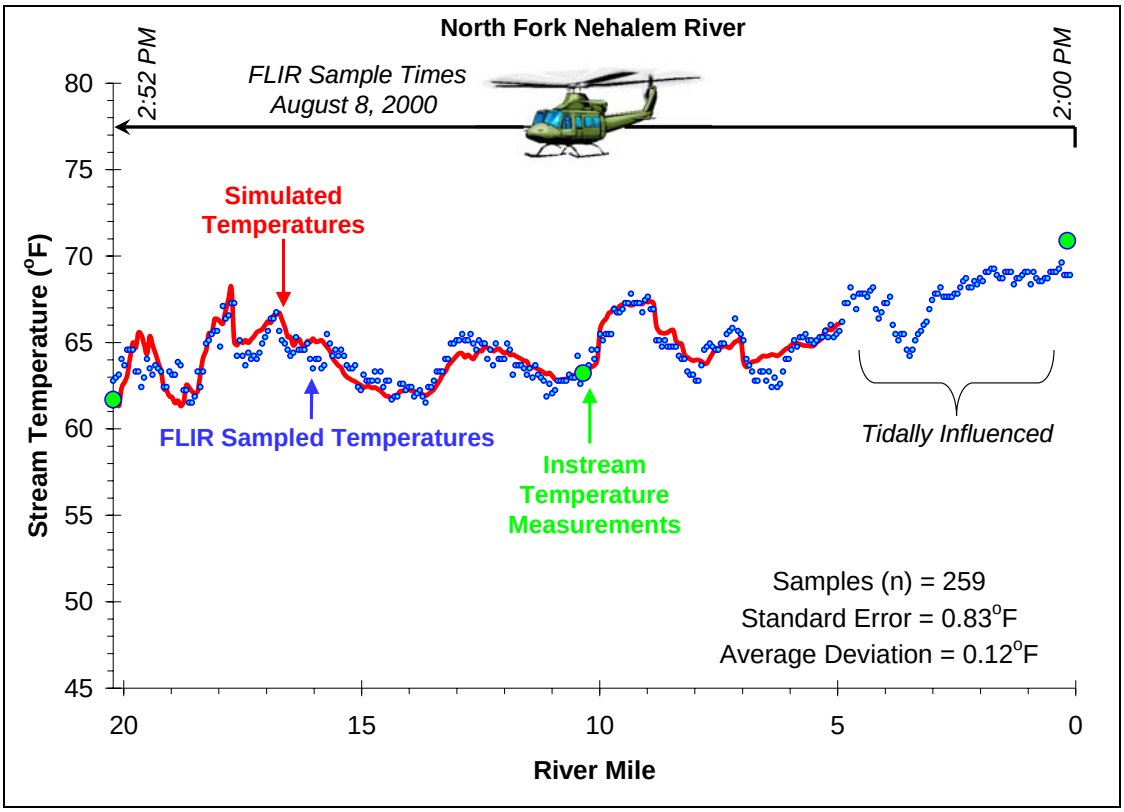

Figure 4-17 (continued). *Stream Temperature Simulation Compared to FLIR Derived Stream Temperatures*

4.3.2 Stream Temperature Simulation Scenarios

4.3.2.1 Nehalem River Stream Temperature Simulations

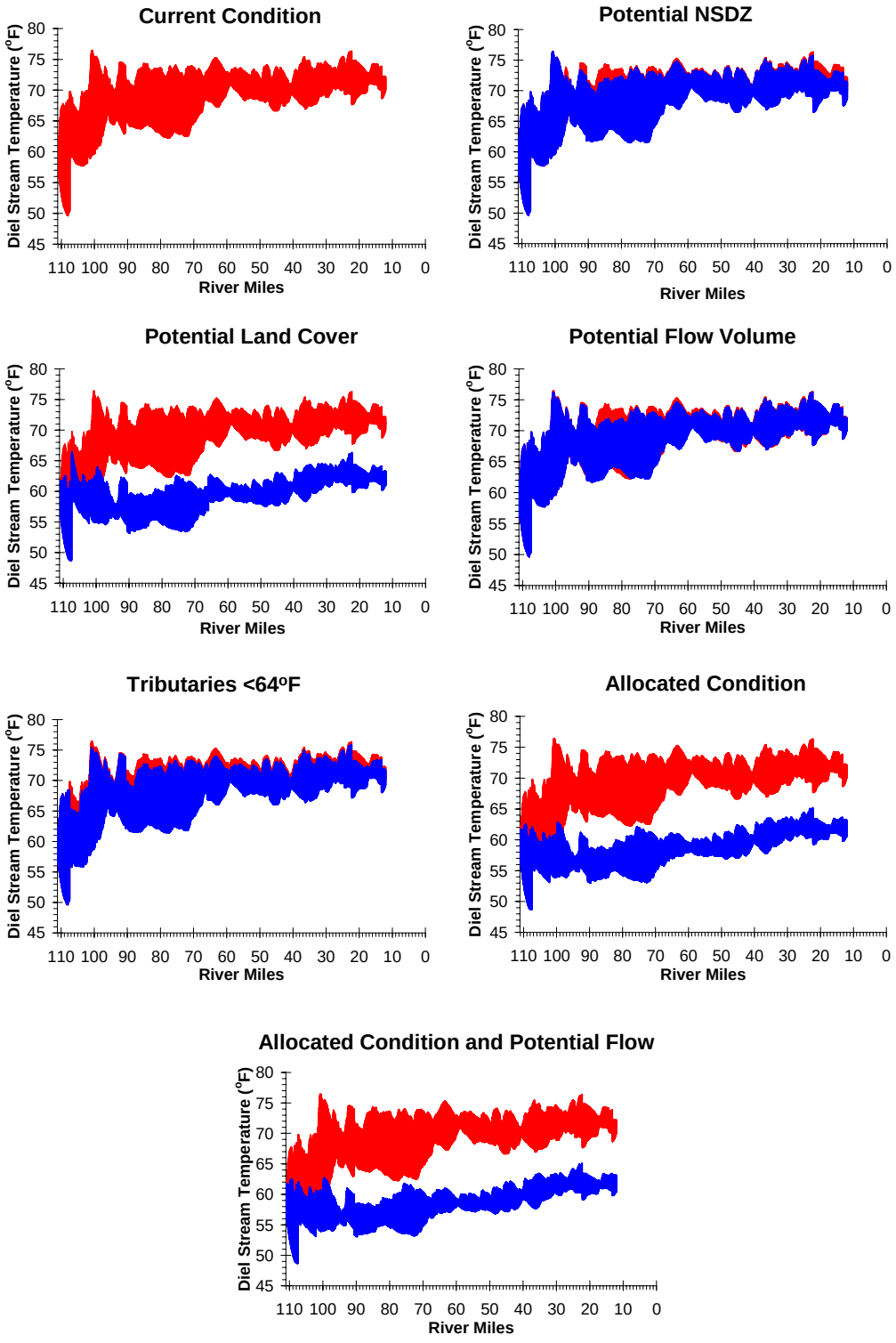

Figure 4-18. *Nehalem River Simulated Stream Temperature Scenarios*

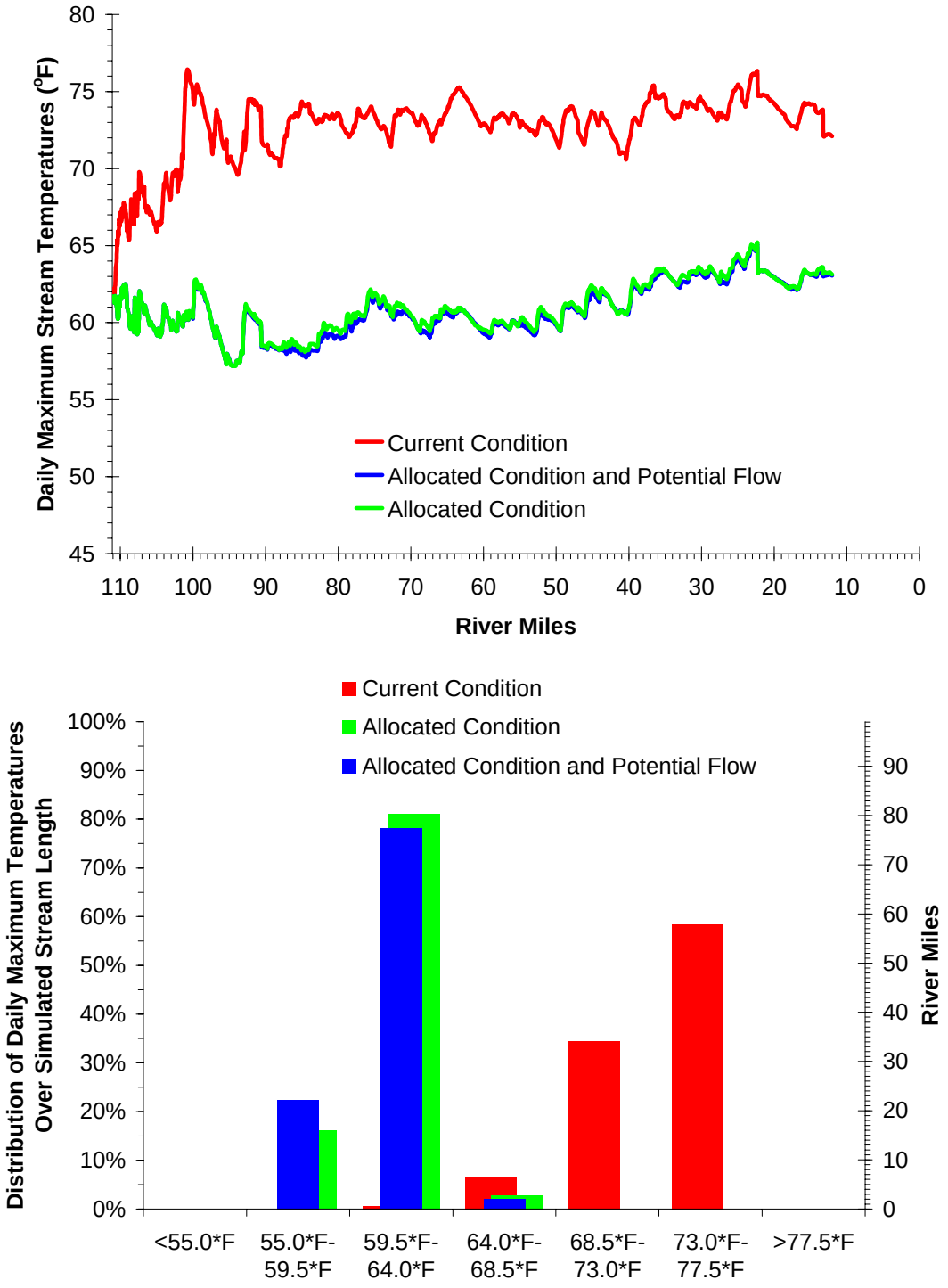

Figure 4-19. *Nehalem River summary of maximum daily simulated potential stream temperatures. Upper chart displays the longitudinal profile of maximum daily stream temperatures. The lower chart is a histogram that shows the distribution of simulated maximum daily stream temperatures for the current condition compared to potential channel width, land cover and flow rate.*

4.3.2.2 Rock Creek Stream Temperature Simulations

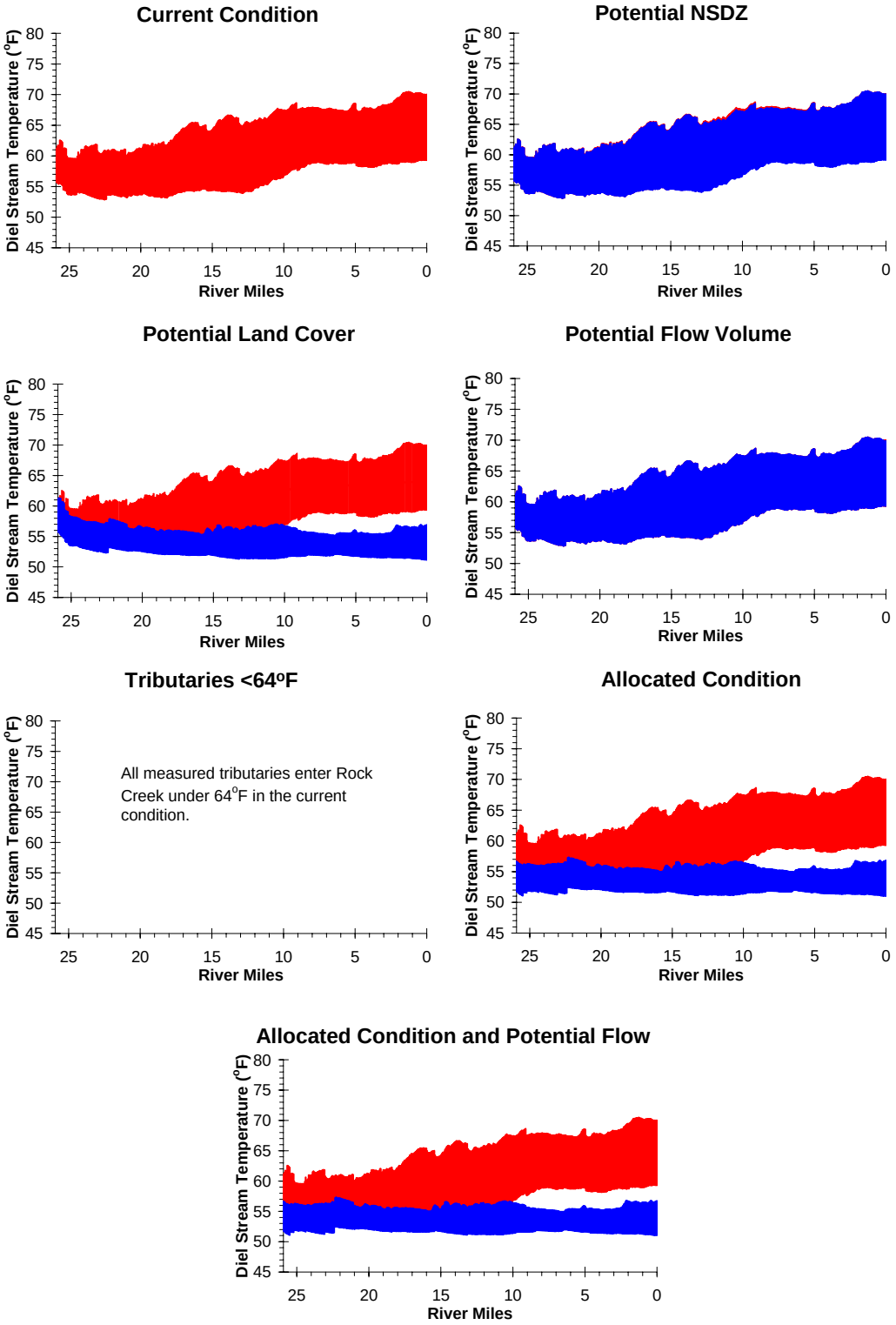

Figure 4-20. *Rock Creek Simulated Stream Temperature Scenarios*

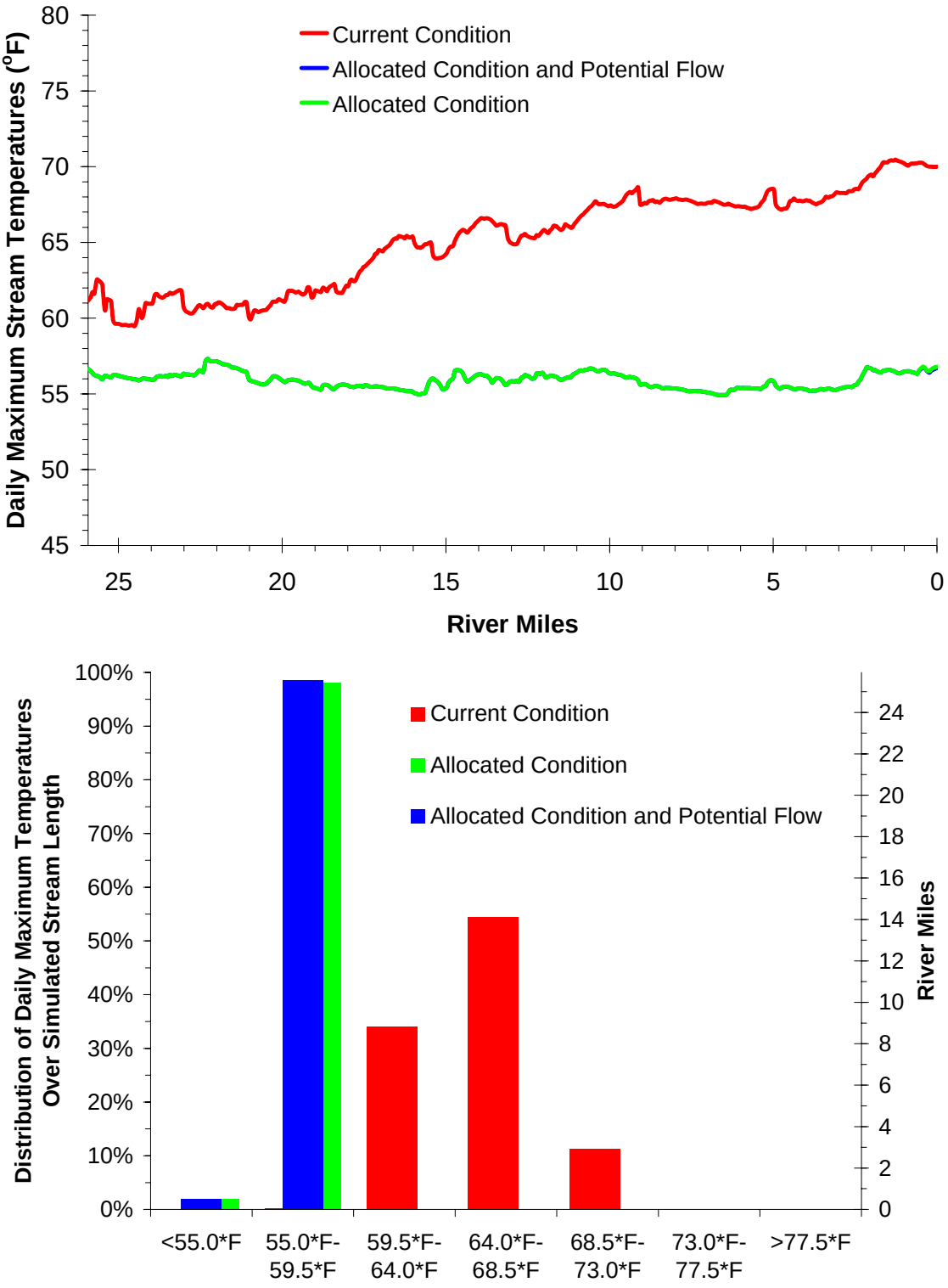

Figure 4-21. *Rock Creek summary of maximum daily simulated potential stream temperatures. Upper chart displays the longitudinal profile of maximum daily stream temperatures. The lower chart is a histogram that shows the distribution of simulated maximum daily stream temperatures for the current condition compared to potential channel width, land cover and flow rate.*

4.3.2.3 Salmonberry River Stream Temperature Simulations

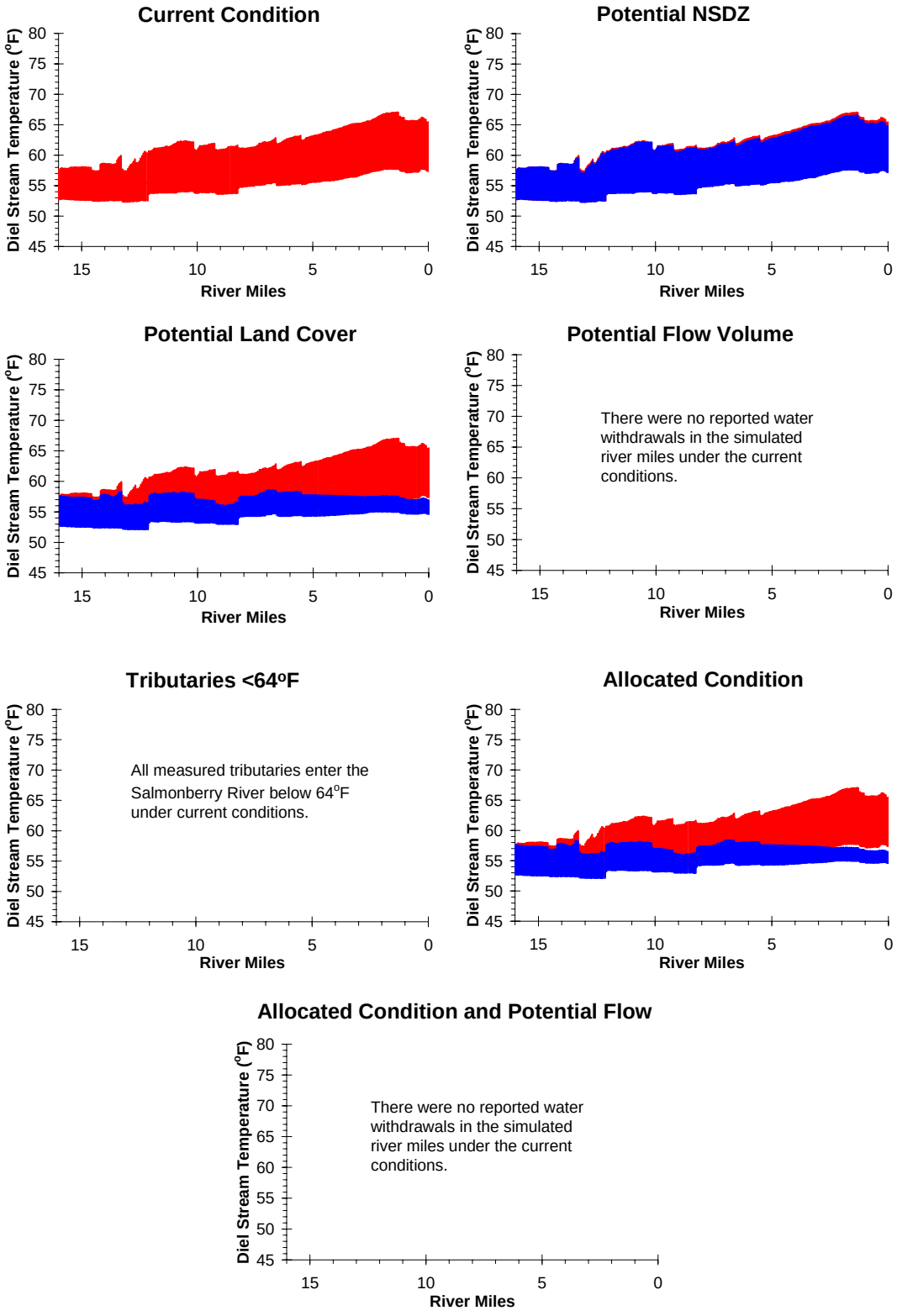

Figure 4-22. *Salmonberry River Simulated Stream Temperature Scenarios*

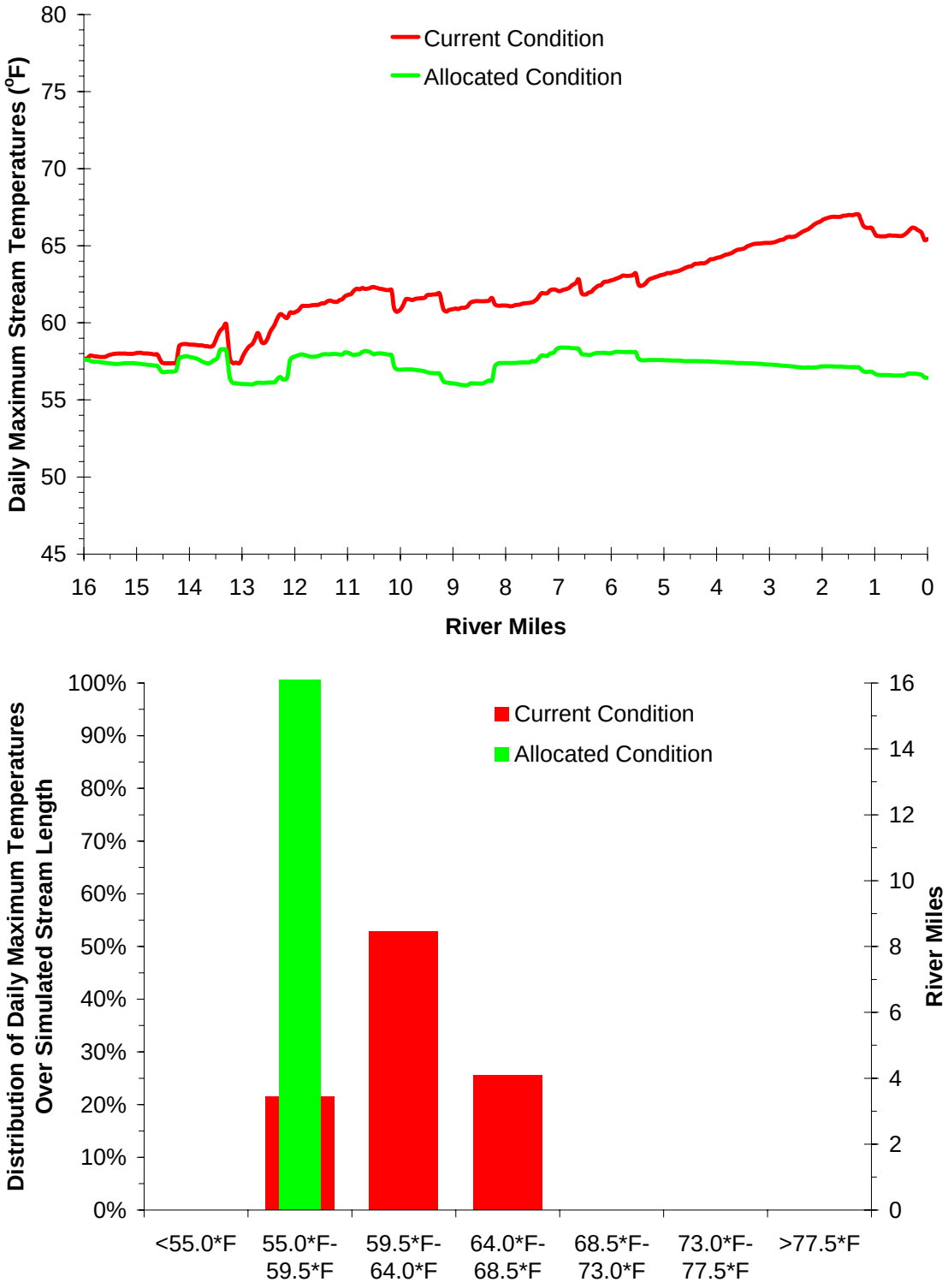

Figure 4-23. *Salmonberry River summary of maximum daily simulated potential stream temperatures. Upper chart displays the longitudinal profile of maximum daily stream temperatures. The lower chart is a histogram that shows the distribution of simulated maximum daily stream temperatures for the current condition compared to potential channel width, land cover and flow rate.*

4.3.2.4 Cook Creek Stream Temperature Simulations

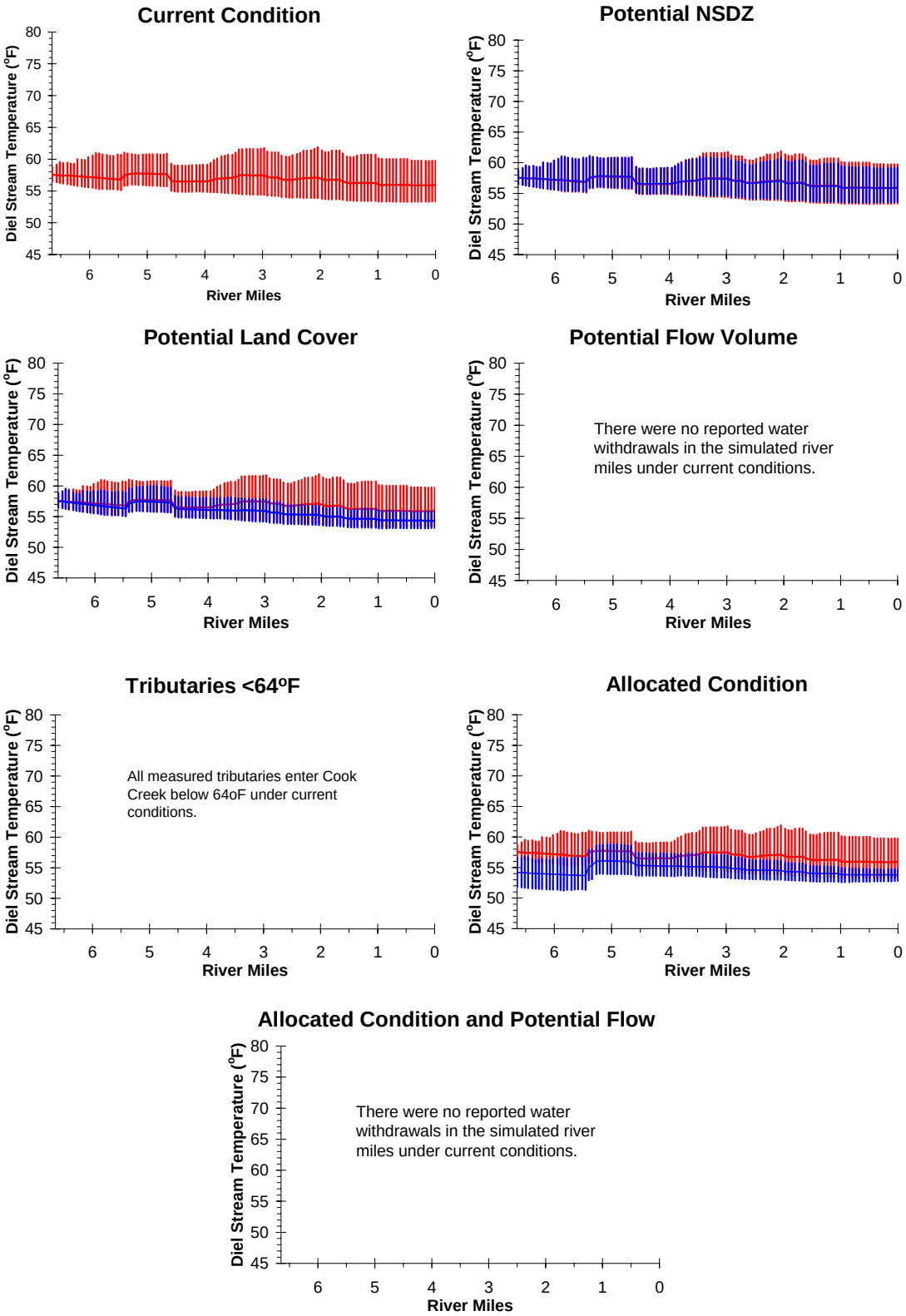

Figure 4-24. *Cook Creek Simulated Stream Temperature Scenarios*

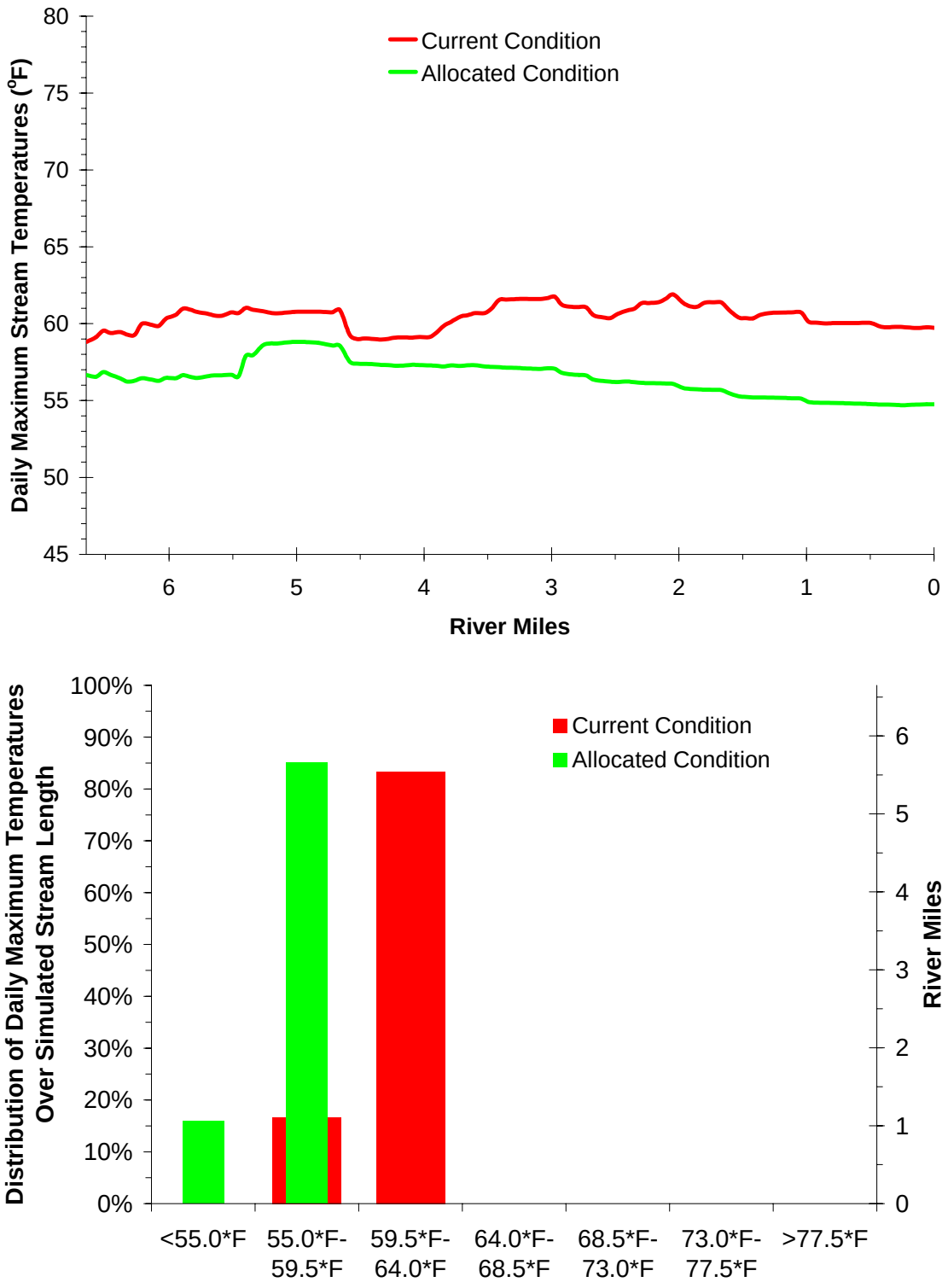

Figure 4-25. *Cook Creek summary of maximum daily simulated potential stream temperatures. Upper chart displays the longitudinal profile of maximum daily stream temperatures. The lower chart is a histogram that shows the distribution of simulated maximum daily stream temperatures for the current condition compared to potential channel width, land cover and flow rate.*

4.3.2.5 North Fork Nehalem River Stream Temperature Simulations

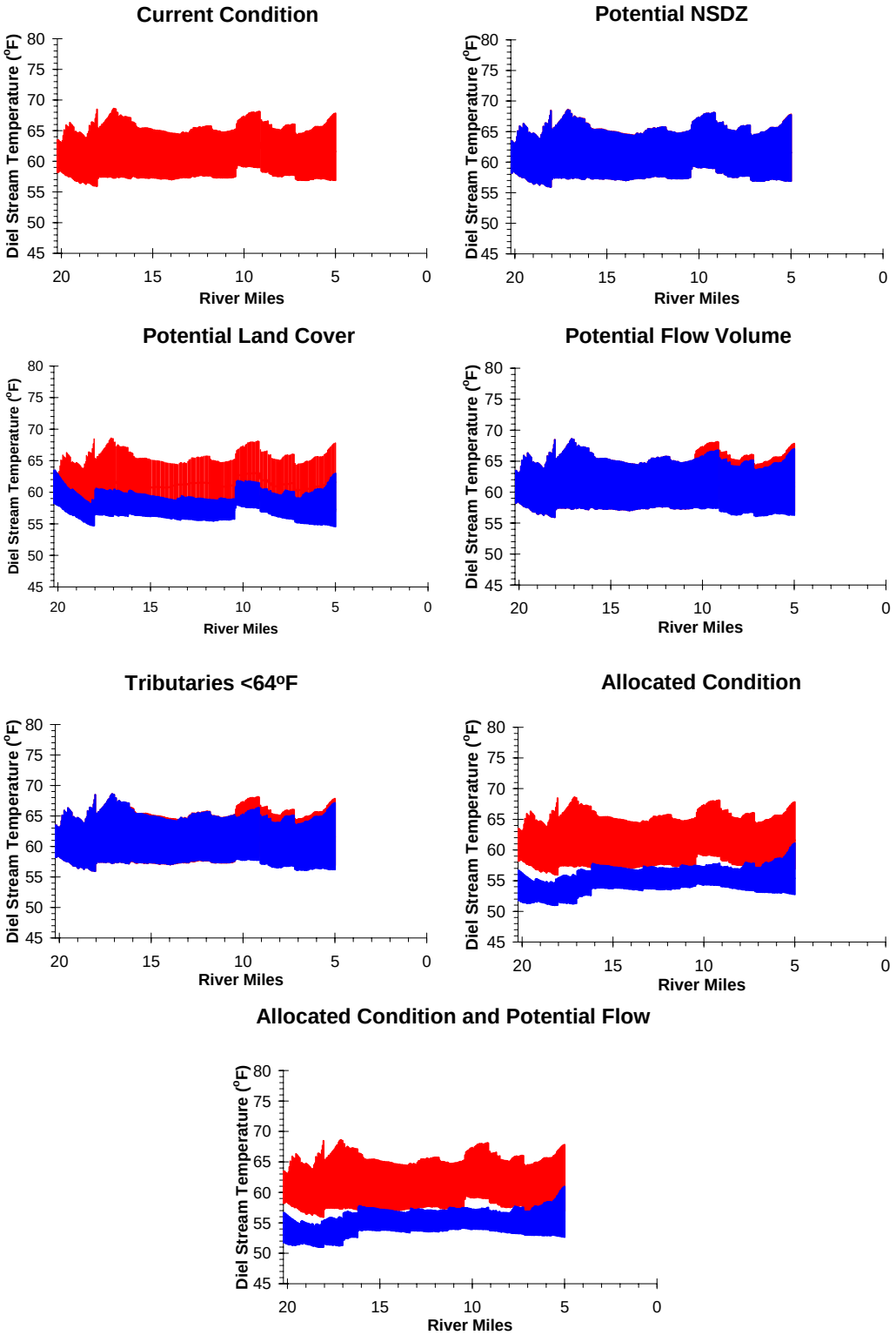

Figure 4-26. *North Fork Nehalem River Simulated Stream Temperature Scenarios*

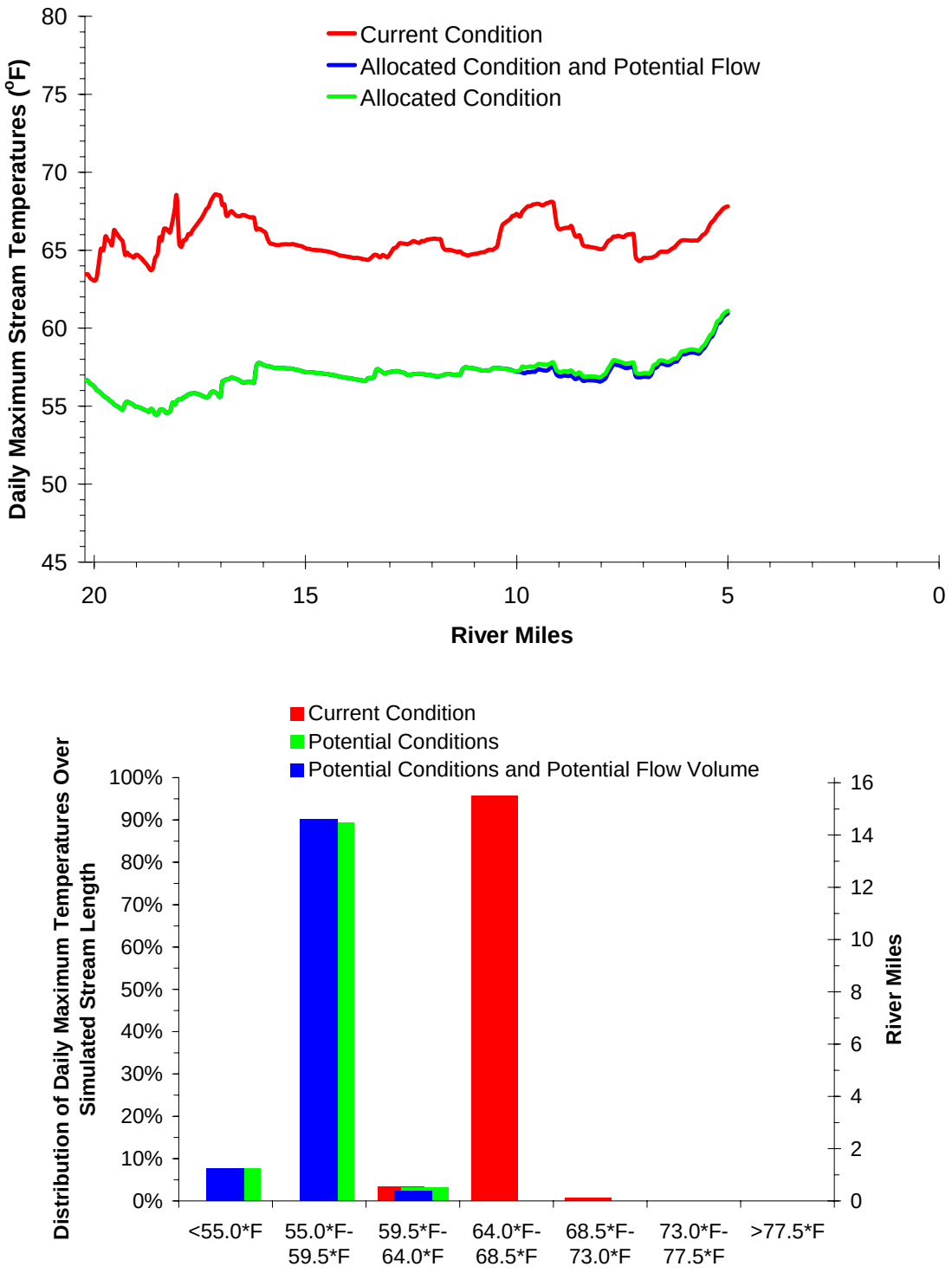

Figure 4-27. *North Fork Nehalem River summary of maximum daily simulated potential stream temperatures. Upper chart displays the longitudinal profile of maximum daily stream temperatures. The lower chart is a histogram that shows the distribution of simulated maximum daily stream temperatures for the current condition compared to potential channel width, land cover and flow rate.*

4.4 DISCUSSION - STREAM TEMPERATURE DISTRIBUTIONS

Maximum daily stream temperature distributions are presented in **Figure 4-28**. Currently 82% of the sampled stream segments (138 river miles) in the Nehalem River Subbasin exceed 64^{o}F. Under potential land cover and channel width (allocated condition), only 2% of the simulated stream segments exceed 64^{o}F. Furthermore, results indicate that 45% of the stream length can achieve maximum daily stream temperatures less than 59.5^{o}F under allocated conditions (system potential conditions).

An overriding emphasis of this analysis is the focus on spatial distributions of stream temperatures in the Nehalem River subbasin. Comparisons of stream temperature distributions capture the variability that naturally exists in stream thermodynamics. Spatial variability is observed in all of the stream segments sampled and analyzed. With the advent of new sampling technologies and analytical tools that include landscape scaled data and computational methodologies, an improved understanding of stream temperature dynamics is emerging (Boyd, 1996, Faux et al. 2001, Torgersen et al., 1995, Torgersen et al., 1999, Torgersen et al., 2001, DEQ 2000a, DEQ 2001a, DEQ2001b, DEQ 2001c). This understanding accommodates spatial and temporal variability that includes departures from biologically derived temperature threshold conditions.

Further, simple conceptual models that focus on a single stream, landscape or atmospheric parameter will fail to capture the interactions of a multitude of parameters that are interrelated. These parameters combine to have complex thermal effects. As an example, temperature simulations demonstrate at a network scale that stream temperature is relatively insensitive to potential land cover conditions. However, when coupled with potential channel width, stream temperatures are highly sensitive to potential land cover. **The results of this analytical effort clearly demonstrate that a comprehensive restoration approach should be developed that focuses on the protection and recovery of land cover and channel morphology.**

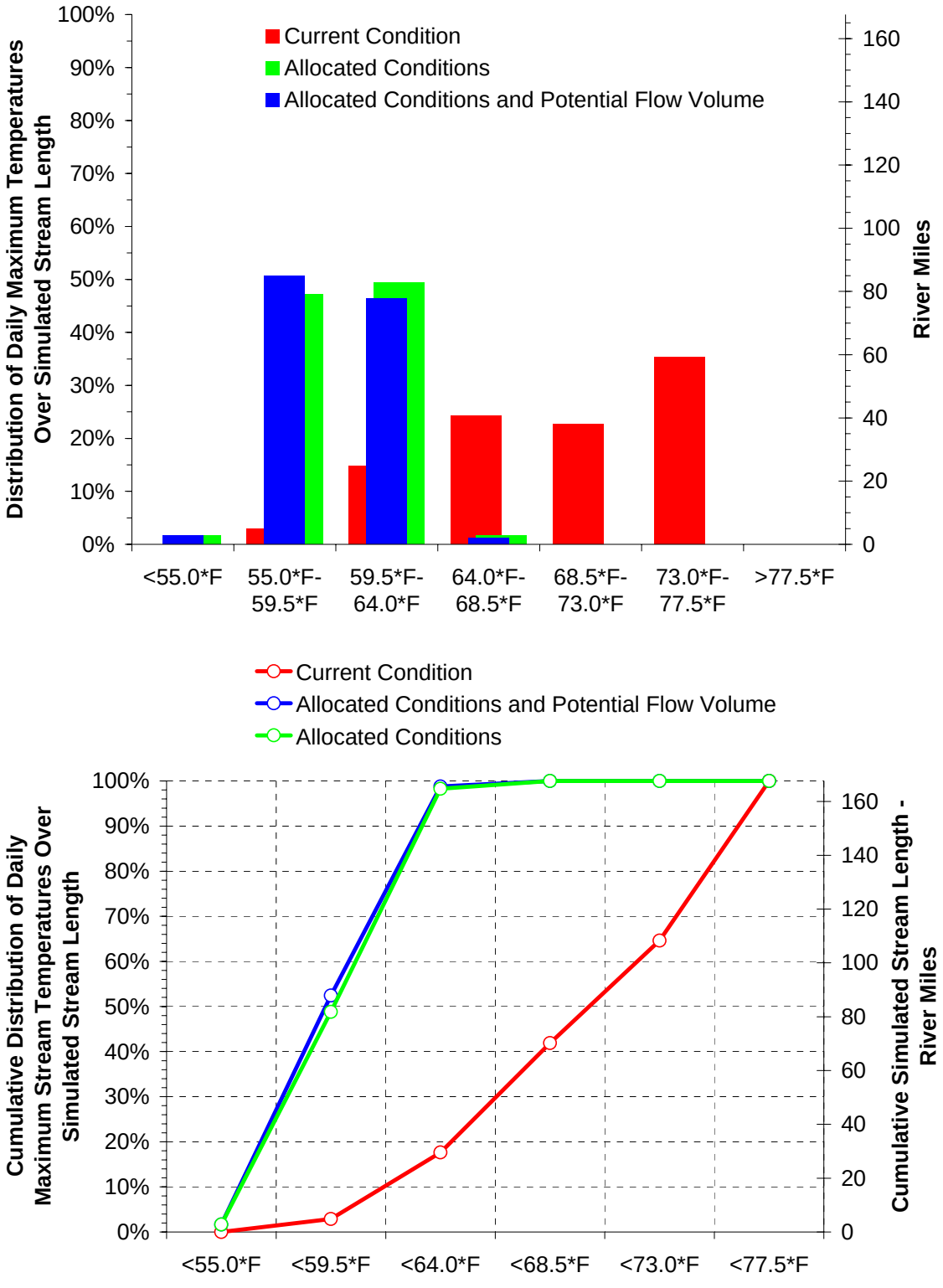

Figure 4-28. *Distributions of maximum daily stream temperatures in the Nehalem River Subbasin stream network (168 river miles) for current and potential conditions.*

LITERATURE CITED

Beschta, R. L., R. E. Bilby, G. W. Brown, L. B. Holtby, and T. D. Hofstra. 1987. Stream temperature and aquatic habitat: Fisheries and forestry interactions. Pages 191-232 in E. O. Salo and T. W. Cundy, eds. *Streamside management: Forestry and fishery interactions*. University of Washington, Institute of Forest Resources, Seattle, USA.

Beschta, R.L. and J. Weatherred. 1984. A computer model for predicting stream temperatures resulting from the management of streamside vegetation. USDA Forest Service. WSDG-AD-00009.

Bowen, I.S. 1926. The ration of heat loss by convection and evaporation from any water surface. Physical Review. Series 2, Vol. 27:779-787.

Boyd, M.S. 1996. Heat Source: stream temperature prediction. Master's Thesis. Departments of Civil and Bioresource Engineering, Oregon State University, Corvallis, Oregon.

Brown, G.W. 1983. Chapter III, Water Temperature. Forestry and Water Quality. Oregon State University Bookstore. Pp. 47-57.

Brown, G.W. 1970. Predicting the effects of clearcutting on stream temperature. Journal of Soil and Water Conservation. 25:11-13.

Brown, G.W. 1969. Predicting temperatures of small streams. Water Resour. Res. 5(1):68-75.

Brown, L.C. and T.O. Barnwell. 1987. The enhanced stream water quality models qual2e and qual2e-uncas: documentation and user manual. U.S. Environmental Protection Agency, Athens, Georgia.

Bureau of Land Management (BLM), 2000. WODIP Guidebook: Western Oregon Digital Image Project. Oregon.

Chen, D.Y. 1996. Hydrologic and water quality modeling for aquatic ecosystem protection and restoration in forest watersheds: a case study of stream temperature in the Upper Grande Ronde River, Oregon. Ph.D. dissertation. University, of Georgia. Athens, Georgia.

Faux, R. N., P. Maus, C. Torgersen, and M. Boyd. 2001. Airborne Thermal Infrared (TIR) Remote Sensing Application to USDA USFS Stream Temperature Monitoring Programs: New Approaches for monitoring thermal variability. USFS Remote Sensing Applications Center, Salt Lake City, Utah.

Hann, D.W. 1997. *Equations for predicting the largest crown width of stand-grown trees in western Oregon.* Forest Research Lab., Oregon State University, Corvallis, Oregon. Research Contribution 17. 14p.

Harbeck, G.E. and J.S. Meyers. 1970. Present day evaporation measurement techniques. J. Hydraulic Division. A.S.C.E., Prceed. Paper 7388.

Ibqal, M. 1983. An Introduction to Solar Radiation. Academic Press. New York. 213 pp.

Leopold, L. B., M. G. Wolman and J. P. Miller. 1964. Fluvial Processes in Geomorphology. Freeman, San Francisco, California. 522 pp.

McArdle, Richard E., Walter H. Meyer, and Donald Bruce. 1930. *The yield of Douglas fir in the Pacific Northwest.* United States Department of Agriculture Technical Bulletin 201. (revised 1949 and 1961).

Oke, T. R. 1978. Boundary Layer Climates. Maethuen and Company, Ltd. London, England. 372 pp.

Oregon Department of Environmental Quality. 2000. Upper Grande Ronde River Subbasin Total Maximum Daily Load.

Oregon Department of Environmental Quality. 2001a. Umatilla River Subbasin Total Maximum Daily Load.

Oregon Department of Environmental Quality. 2001b. Tualatin River Subbasin Total Maximum Daily Load.

Oregon Department of Environmental Quality. 2001c. Tillamook Bay Drainage Total Maximum Daily Load.

Oregon Water Resources Department. 2001. Water rights information system (WRIS) and points of diversion (POD) databases. http://www.wrd.state.or.us/.

Park, C. 1993. SHADOW: stream temperature management program. User's Manual v. 2.3. USDA Forest Service. Pacific Northwest Region.

Parker, F.L. and P.A. Krenkel. 1969. Thermal pollution: status of the art. Rep. 3. Department of Environmental and Resource Engineering, Vanderbilt University, Nashville, TN.

Richards, F. J. 1959. A flexible growth function for empirical use. J. Exp. Botany 10:290–300.

Rishel, G.B., Lynch, J.A. and E.S. Corbett.. 1982. Seasonal stream temperature changes following forest harvesting. J. Environ. Qual. 11:112-116.

Rosgen, D. 1996. Applied River Morphology. Wildland Hydrology. Pagosa Springs, Colorado.

Sattterland, D.R. and P.W. Adams. 1992. Wildland Watershed Management. 2nd edition. John Wiley and Sons, Inc., New York.

Sellers, W.D. 1965. Physical Climatology. University of Chicago Press. Chicago, IL. 272 pp.

Sinokrot, B.A. and H.G. Stefan. 1993. Stream temperature dynamics: measurement and modeling. Water Resour. Res. 29(7):2299-2312.

Torgersen, C.E., D.M. Price, H.W. Li, and B.A. McIntosh. 1995. Thermal refugia and chinook salmon habitat in Oregon: Applications of airborne thermal videography. Proceedings of the 15th Biennial Workshop on Color Photography and Videography in Resource Assessment, Terre Haute, Indiana. May, 1995. American Society for Photogrammetry and Remote Sensing.

Torgersen, C. E., D. M. Price, H. W. Li, and B. A. McIntosh. 1999. Multiscale thermal refugia and stream habitat associations of chinook salmon in northeastern Oregon. *Ecological Applications* 9: 301-319.

Torgersen, C.E., R. Faux, B.A. McIntosh, N. Poage, and D.J. Norton. 2001. Airborne thermal remote sensing for water temperature assessment in rivers and streams. *Remote Sensing of Environment* 76(3): 386-398.

Whitney, S. 1985. *Western Forests*. National Audubon Society Nature Guides, Chanticleer Press, Inc., New York.

Wunderlich, T.E. 1972. Heat and mass transfer between a water surface and the atmosphere. Water Resources Research Laboratory, Tennessee Valley Authority. Report No. 14, Norris Tennessee. Pp 4.20.